The bomb ^{14}C transient in the Pacific Ocean

Keith B. Rodgers [1]

Lamont-Doherty Earth Observatory of Columbia University, Palisades, New York

Daniel P. Schrag

Department of Earth and Planetary Sciences, Harvard University, Cambridge, Massachusetts

Mark A. Cane and Naomi H. Naik

Lamont-Doherty Earth Observatory of Columbia University, Palisades, New York

Abstract. A modeling study of the bomb ^{14}C transient is presented for the Pacific Ocean. A primitive equation ocean circulation model has been configured for a high-resolution domain that accounts for the Indonesian Throughflow (ITF). Four separate runs were performed: (1) seasonal forcing with 20 Sv of ITF transport, (2) seasonal forcing with 10 Sv of ITF transport, (3) seasonal forcing with no ITF transport, and (4) interannual forcing with 15 Sv of ITF transport. This study has two main objectives. First, it is intended to describe the time evolution of the bomb ^{14}C transient. This serves as a tool with which one can identify the physical processes controlling the evolving bomb ^{14}C distribution in the Pacific thermocline and thus provides an interpretive framework for the database of $\Delta^{14}C$ measurements in the Pacific. Second, transient tracers are applied to the physical oceanographic problem of intergyre exchange. This is of importance in furthering our understanding of the potential role of the upper Pacific Ocean in climate variability. We use bomb ^{14}C as a dye tracer of intergyre exchange between the subtropical gyres and the equatorial upwelling regions of the equatorial Pacific. Observations show that while the atmospheric $\Delta^{14}C$ signal peaked in the early to mid-1960s, the $\Delta^{14}C$ levels in the surface water waters of the subtropical gyres peaked near 1970, and the $\Delta^{14}C$ of surface waters in the equatorial Pacific continued to rise through the 1980s. It is shown that the model exhibits skill in representing the large-scale observed features observed for the bomb ^{14}C transient in the Pacific Ocean. The model successfully captures the basin-scale inventories of bomb ^{14}C in the tropics as well as in the extratropics of the North Pacific. For the equatorial Pacific this is attributed to the model's high meridional resolution. The discrepancies in the three-dimensional distribution of bomb ^{14}C between the model and data are discussed within the context of the dynamical controls on the $\Delta^{14}C$ distribution of bomb ^{14}C in the Pacific.

1. Introduction

A high-resolution primitive equation ocean model has been used to simulate the bomb ^{14}C transient in the Pacific Ocean between 1955 and 1980. Over the period since the peak in atmospheric testing of nuclear weapons in the 1950s and 1960s, ^{14}C has behaved essentially as a dye tracer within the directly ventilated layers of the Pacific thermocline. The primary pathway by which bomb ^{14}C reaches the subsurface layers of the subtropical and tropical Pacific is through subduction in the subtropical gyres. Our investigation focuses primarily on bomb ^{14}C as a tracer of intergyre exchange between the subducting regions of the extratropics and the equatorial pycnocline of the Pacific Ocean.

Recently, it has been proposed that intergyre exchange of thermal anomalies between the subducting regions of the extratropical Pacific and the equatorial pycnocline provides an advective means of changing the temperature of the upwelling water in the eastern equatorial Pacific [*Deser et al.*, 1996; *Gu and Philander*, 1997; *Zhang et al.*, 1998]. The effectiveness of this mechanism will depend on the amplitude of diapycnal

[1]Now at Max-Planck-Institut für Meteorologie, Hamburg, Germany.

Paper number 1999JC900228.
0148-0227/99/1998JC900228$09.00

fluxes associated with intergyre exchange between the subtropics and the equatorial thermocline. Prebomb $\Delta^{14}C$ levels recorded by corals in the equatorial upwelling region suggest that significant amounts of water from below the directly ventilated thermocline are entrained into the equatorial upwelling [*Toggweiler et al.*, 1991]. Although prebomb $\Delta^{14}C$ can provide us with important qualitative clues as to the extent of dilution associated with intergyre exchange, other tracers are needed to provide a quantitative assessment.

This study extends our earlier process study of the dynamical mechanisms controlling seasonal variability of sea surface $\Delta^{14}C$ in the equatorial Pacific [*Rodgers et al.*, 1997]. There we identified seasonal variability in the surface currents of the Pacific Ocean as the dynamical mechanism responsible for the high seasonal $\Delta^{14}C$ variability during the 1970s and 1980s recorded by corals. Given that the boundaries of the Pacific domain used in that study were 30°N and 30°S, we were unable to represent the subtropical subduction process at the polar end of the shallow meridional cell within the thermocline.

$\Delta^{14}C$ has proven useful as a tracer of ocean circulation on timescales ranging from the seasonal cycle [*Moore et al.*, 1997; *Rodgers et al.*, 1997; and *Guilderson et al.*, 1998; and *Guilderson and Schrag*, 1998] to the ventilation age of the deep Pacific [*Stuiver et al.*, 1983]. Our purpose here is to demonstrate the utility of $\Delta^{14}C$ as a tracer of upper ocean processes on El Niño-Southern Oscillation (ENSO) to decadal timescales in the Pacific Ocean. As the timescale of radioactive decay for ^{14}C isotopes is more than 2 orders of magnitude larger than either the timescale of Pacific thermocline circulation or the bomb transient, we can ignore radioactive decay as a sink of ^{14}C in our treatment of bomb ^{14}C as a perturbation to the prebomb $\Delta^{14}C$ in our analysis. However, it is important to describe first the observed prebomb distribution of $\Delta^{14}C$ since it has much to teach us about circulation in the upper Pacific Ocean.

Before anthropogenic perturbations, $\Delta^{14}C$ levels in the ocean and atmosphere were approximately in steady state. By definition the $\Delta^{14}C$ of the prebomb atmosphere was zero per mil. It is generally assumed that the natural sources were roughly balanced by natural sinks, with the principal sink of ^{14}C being radioactive decay within the ocean, and the principal source being spallation in the upper atmosphere. Deep waters in the Pacific Ocean have a radiocarbon content that is ~20% (i.e., 200‰) less than that of the preanthropogenic atmosphere, which, given the 5730 year half life of ^{14}C, yields an apparent ventilation age of 1500 years.

Within the Pacific thermocline, measurements collected in the open ocean during the 1950s [*Linick*, 1978], in addition to $\Delta^{14}C$ values recorded by corals [*Druffel*, 1987], show that the range of $\Delta^{14}C$ was between -70 and -40‰ for the surface ocean and upper thermocline. Lateral and vertical gradients in the thermocline and surface ocean were of order 30‰. The bomb ^{14}C transient introduced lateral and vertical gradients in the sea surface and thermocline distribution of $\Delta^{14}C$, which were an order of magnitude larger than the prebomb gradients.

Several different ocean models have previously been used with a global domain to study the bomb ^{14}C transient [*Toggweiler et al.*, 1989b; *Duffy et al.*, 1995]. In their discussion of the bomb $\Delta^{14}C$ distribution for the upper Pacific Ocean these studies have focused on the model's $\Delta^{14}C$ distribution in the northern and southern subtropics. In particular, they compared their simulated distribution of $\Delta^{14}C$ in the subtropical gyres with Geochemical Ocean Sections Survey (GEOSECS) data. However, these coarse-resolution models cannot give a satisfactory representation of equatorial thermocline ventilation as they do not represent the critical scales of circulation in the equatorial Pacific.

In addition, the models tend to be overly diffusive. They are typically tuned in such a way that the amplitude of the global-scale thermohaline circulation produces a $\Delta^{14}C$ distribution that matches GEOSECS measurements of the prebomb $\Delta^{14}C$ distribution in the deep Pacific. Such models achieve the apparent 1500 year ventilation timescale for the deep Pacific, and thus the observed deep-Pacific $\Delta^{14}C$ values of roughly -250‰, at the expense of an overly diffuse thermocline. The thermocline distribution of bomb ^{14}C generated by such models is far from satisfactory.

In configuring our model domain for the current study we specifically chose high vertical resolution in the upper several hundred meters, high meridional resolution within the equatorial thermocline, and high zonal resolution for the western boundary currents in order to achieve model skill for the thermocline circulation associated with intergyre exchange.

2. $\Delta^{14}C$ As a Tracer of Ocean Circulation

$\Delta^{14}C$ is defined as the per mil deviation of the ratio of the isotopic species ^{14}C and ^{12}C in CO_2 from the ratio in the preanthropogenic atmosphere with a mass-dependent fractionation using the stable isotope ^{13}C. The equilibration timescale for carbon isotopes between the mixed layer and the overlying atmosphere is of order 10 years, and this is due to the buffering effect of dissolved inorganic carbon in the ocean.

The atmospheric testing of hydrogen bombs during the 1950s and early 1960s produced sufficient ^{14}C to increase atmospheric $\Delta^{14}C$ levels in the atmosphere by more than 50%. Figure 1 shows a time series of atmospheric $\Delta^{14}C$ between 1955 and 1990 [*Broecker et al.*, 1995]. The $\Delta^{14}C$ signal is separated into three different latitude bands. During the early and mid-1960s the atmospheric $\Delta^{14}C$ signal is largest in the Northern Hemisphere, which is due to the fact that the majority of the aboveground hydrogen bomb tests were conducted

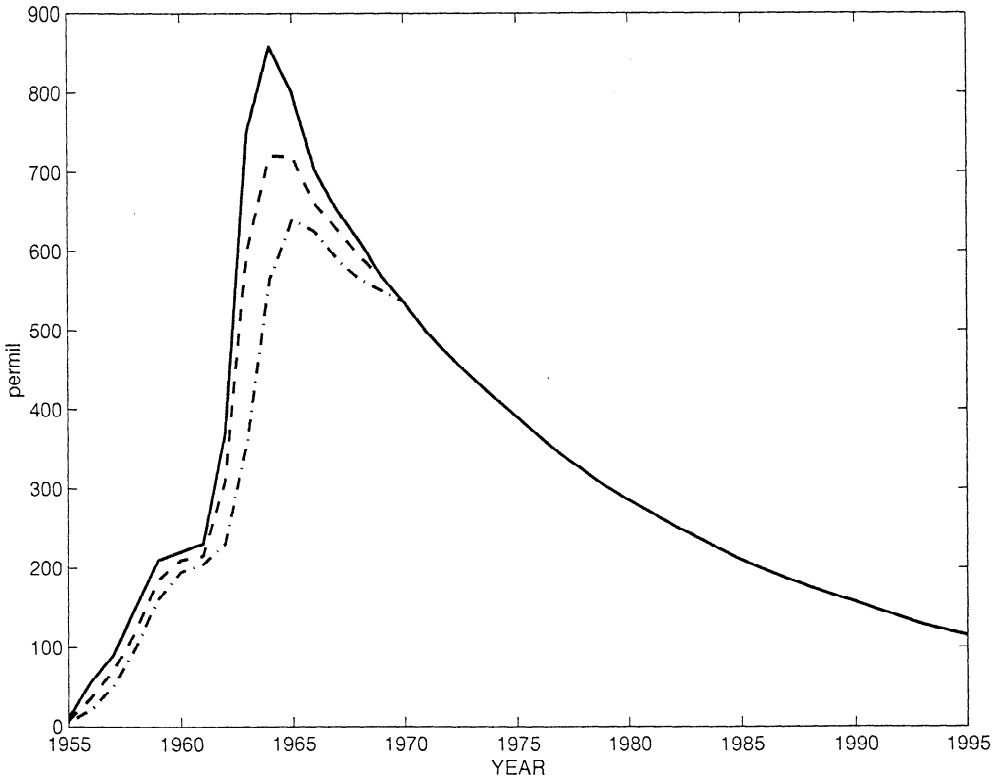

Figure 1. Time series of $\Delta^{14}C$ values for the atmosphere, separated into three latitude bands [Broecker et al., 1995]. The solid line is for latitudes north of 20°N, the dashed line for latitudes between 20°N and 20°S, and the dashed-dotted line for latitudes south of 20°S.

there. At the time of peak atmospheric $\Delta^{14}C$ values in 1964 and 1965 the interhemispheric gradient within the atmosphere was more than 200‰. Upon entering the ocean this bomb ^{14}C produced large lateral and vertical gradients in $\Delta^{14}C$ within the surface ocean and the thermocline. As a result of this, the bomb ^{14}C signal overwhelmed the gradients present in the prebomb ocean, and thus bomb ^{14}C in the upper ocean serves as a dye tracer that tagged subducting thermocline waters with high-$\Delta^{14}C$ values.

3. Model Experiment Description

3.1. The Circulation Model

The model used for this study is the primitive equation Lamont Ocean-Atmospheric Mixed Layer Model (LOAM), which is a descendent of the *Gent and Cane* [1989] model. Model calculations are performed on an A grid, and a level vertical grid is used, with realistic bathymetry and a barotropic solver [*Naik et al.*, 1995]. The model domain extends meridionally from 68°S to 62°N and zonally from 100.5° to 300°E. The total number of vertical layers is 30, with 15 of these layers in the upper 300 m. The meridional resolution along the equator is ~0.33°, tapering off to almost 2.5° in the extratropics. The zonal resolution is almost 2° in the extratropics but is stretched to slightly less than 1° in the western boundary regions as well as in the vicinity of the Peru upwelling. This is the same grid spacing we used for our study of the effect of the Indonesian Throughflow (ITF) on equatorial thermocline ventilation [*Rodgers et al.*, 1999]. There we found that the mixing ratio of northern to southern component water in the equatorial thermocline is in best agreement with the value inferred from equatorial salinity measurements when the imposed ITF transport is between 10 and 20 Sv. The same two domains used for that study are again used here. They differ in that the first domain does not allow for flow between the Pacific and Indian Oceans through the Indonesian Straits separating New Guinea and the Asian continent, whereas the second domain does allow for flow through the Indonesian Straits.

Vertical mixing is achieved using the parameterization of *Pacanowski and Philander* [1981] in addition to convective adjustment. Lateral mixing of temperature and salinity (as well as passive tracers) is achieved using a modified version of the *Griffies* [1998] implementation of the ocean eddy mixing parameterization of *Gent and McWilliams* [1990]. The eddy transfer coefficient used with the Gent and McWilliams parameterization varies linearly with model resolution because of grid stretching. The minimum value for the eddy transfer coefficient is ~200 m^2 s^{-1}, and the maximum value is

~1600 m^2 s^{-1}. A fourth-order Shapiro filter [*Shapiro*, 1970] is used to remove two gridpoint waves in the momentum equations. In addition, a lateral diffusivity of 1500 m^2 s^{-1} has been used with the momentum equations in order to tune the structure of the equatorial undercurrent (EUC), which is too strong under the influence of the Shapiro filter alone.

Surface heat fluxes are calculated using the atmospheric mixed layer model of *Seager et al.* [1995], with monthly climatologies used for surface solar radiation [*Li and Leighton*, 1993], fractional cloudiness [*Rossow and Schiffer*, 1991], and surface winds within the AML [*Gibson et al.*, 1977]. A storm track parameterization of is now included in the AML model, and a description of this as well as its effect on the model's simulation of extratropical wintertime sea surface temperatures (SSTs) is described by *Hazelage et al.* [1999]. The boundary condition used for sea surface salinity is relaxation to the Levitus monthly climatology in the surface layer with a timescale of 1 month.

3.2. Description of Experiments

A total of four model runs were performed for this study. They differ in the choice of wind stress wind forcing (seasonal versus interannual wind stress data set of daSilva et al. [1994]), as well as in their representation of the Indonesian Throughflow. These differences are summarized in Table 1. A simple naming convention is used to distinguish between the runs: S is used to denote runs forced with seasonally varying winds and is followed by a number representing the net imposed ITF transport in Sverdrups; likewise, I15 indicates interannual wind forcing with 15 Sv of imposed ITF. The set of runs consists of S0, S10, S20, and I15; S10 is the control run.

Run S0 does not allow for any Indonesian Throughflow, and is forced at the sea surface with the seasonally varying monthly wind stress climatology of *daSilva et al.* [1994]. The other three experiments use a domain that allows for flow through the Indonesian Straits connecting the Pacific and Indian Oceans. Run S10, which we define to be the control run, imposes a time-invariant barotropic flow of 10 Sv through the Indonesian Straits, and run S20 imposes 20 Sv of barotropic flow. Both S10 and S20 are forced at the sea surface with seasonal wind stress climatology of *daSilva et al.* [1994].

Run I15 imposes 15 Sv of ITF transport and is forced at the sea surface with the *daSilva et al.* [1994] interannually varying monthly wind stress climatology. The wind stress anomalies contained in the data set will generate interannual variability in ocean circulation. Although this global data set contains entries for each month since the beginning of 1945, the number of wind observations in the western equatorial Pacific is small before the 1970s. For I15 the imposed transport for 15 Sv was motivated by the *Rodgers et al.* [1999] finding that only when the mean ITF transport is between 10 and 20 Sv does the ratio of Southern to Northern Hemispheric thermocline water in the equatorial undercurrent increase to a value greater than unity.

For each of the runs the model is initialized with *Levitus and Boyer* [1994] temperature and salinity fields, and then spun up for 10 years in robust diagnostic mode [*Sarmiento and Bryan*, 1982]. A restoring timescale for temperature and salinity used within the thermocline is 180 days during this period. The model is then restarted in 1955, at which point the transient tracer fields are initialized, without any restoring of subsurface temperature and salinity fields.

4. Tracer Formulation

The treatment of $\Delta^{14}C$ as a tracer follows that of *Toggweiler et al.* [1989a]. The gas exchange formulation of *Broecker et al.* [1985] is used in conjunction with the atmospheric $\Delta^{14}C$ time series of *Broecker et al.* [1995] (shown in Figure 1) to represent fluxes at the sea surface. The wind speed climatology used is from the European Centre for Medium-Range Weather Forecasts (ECMWF) analysis [*Gibson et al.*, 1977]. $\Delta^{14}C$ is initialized using the empirically derived relationship between thermocline SiO_2 and prebomb $\Delta^{14}C$ of *Broecker et al.* [1995],

$$\Delta^{14}C = -70 - SiO_2, \quad (1)$$

and the gridded Levitus SiO_2 distribution of *Levitus and Boyer* [1994].

5. Model Results: Bomb ^{14}C Transient for the Control Case

First, the results for the seasonally forced control run (case S10), for which 10 Sv of ITF were imposed, are presented. Our purpose here is to describe the three-dimensional structure of the bomb ^{14}C transient moving through the upper ocean between 1955 and 1985. This section begins with a description of the the evolving sea surface $\Delta^{14}C$ distribution before moving on to the evolution of the thermocline distribution of $\Delta^{14}C$.

5.1. Sea Surface $\Delta^{14}C$

The annual mean sea surface $\Delta^{14}C$ at 5 year intervals from 1960 to 1985 are shown in Figures 2a-2f. By 1960 a relative maximum of high $\Delta^{14}C$ has developed at the sea surface in the subtropical and subpolar regions, with low $\Delta^{14}C$ values in the equatorial region. The meridional gradient in sea surface $\Delta^{14}C$ between the tropics and the extratropics increases significantly by 1965 (Figure 2b).

By 1965 the atmospheric $\Delta^{14}C$ has already begun to drop, as can be seen in Figure 1, although it is still in excess of 500‰ at all latitudes. The maximum sea surface $\Delta^{14}C$ at this time is slightly larger than 300‰, and thus the gradient in $\Delta^{14}C$ across the sea surface is still quite large. The year 1965 is also characterized by a hemispheric asymmetry in the distribution of sub-

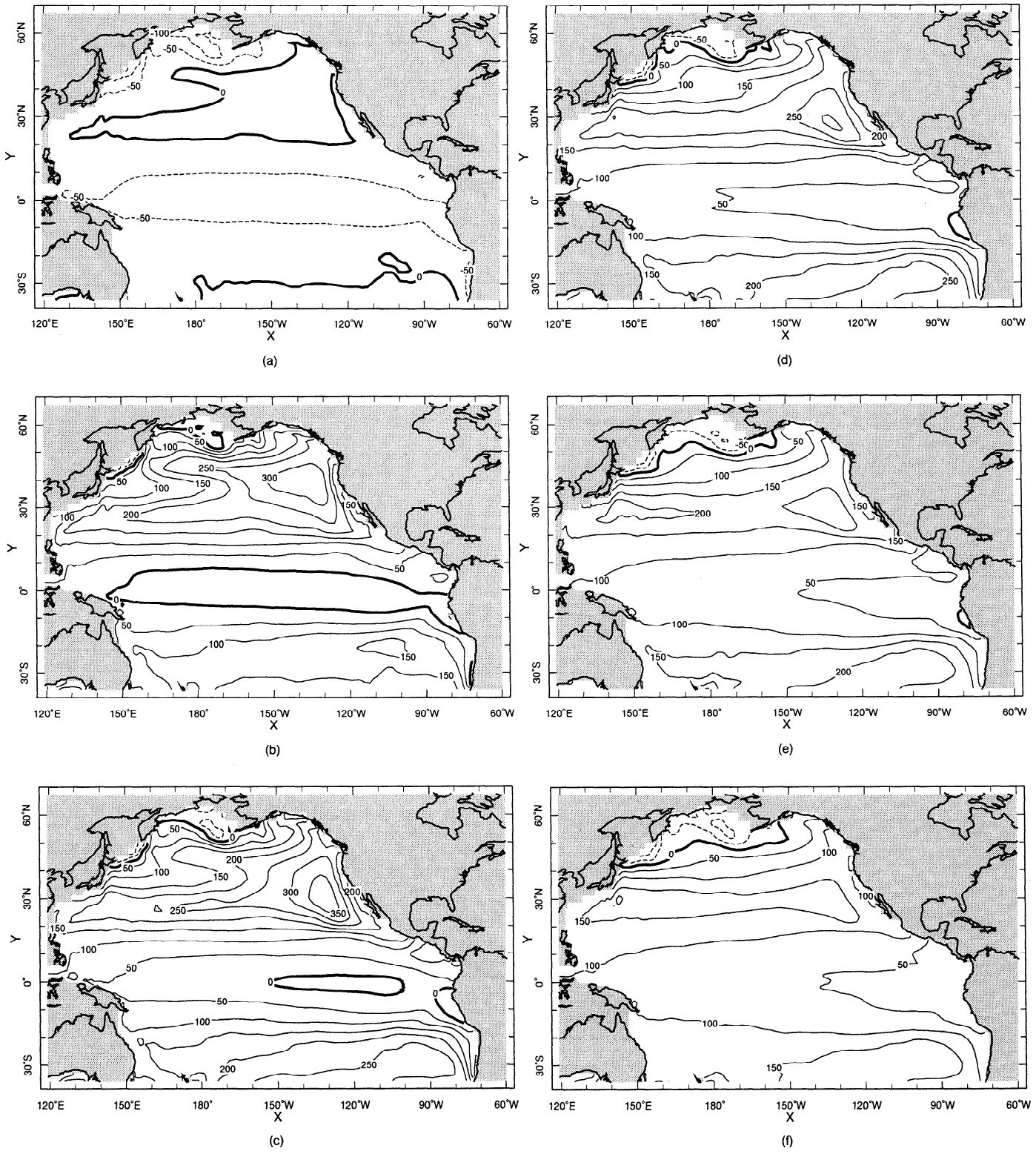

Figure 2. Annual mean sea surface $\Delta^{14}C$ in (a) 1960, (b) 1965, (c) 1970, (d) 1975, (e) 1980, and (f) 1985 for the control case S10.

tropical sea surface $\Delta^{14}C$ about the equator. In 1965 the maximum values in the Northern Hemispheric subtropics are in excess of 100‰ larger than the values in the Southern Hemispheric subtropics, reflecting the large meridional gradient in atmospheric $\Delta^{14}C$ that existed in the early 1960s (Figure 1). Note too that the zonal gradients across the subtropics of the Northern Hemisphere are significantly larger than those across the subtropics of the Southern Hemisphere.

By 1970 the surface $\Delta^{14}C$ values in the subtropics have increased, with the amount of increase being larger for the Southern Hemispheric subtropics than for

the Northern Hemispheric subtropics. Although atmospheric Δ^{14}C values peaked in the mid-1960s, 1970 represents the time of maximum sea surface Δ^{14}C in the subtropics. The lag between the peaks is due to the 5-10 year air-sea equilibration timescale for Δ^{14}C isotopes. In the eastern equatorial Pacific, regions with Δ^{14}C values of $<0‰$ persist in the upwelling region between 160° and 100°W, as well as in the region of upwelling off the coast of Peru.

Subtropical sea surface Δ^{14}C values have dropped between 1970 and 1975 (Figure 2e), whereas values in the equatorial Pacific have risen. The region of negative sea surface Δ^{14}C values in the tropics is now confined to the Peru upwelling region.

5.2. Thermocline Distribution of Δ^{14}C

In Figure 3 we consider the distribution of Δ^{14}C as it evolves across 32°N in 1960, 1970, and 1980. The distributions shown in Figure 3 represent snapshots on January 1 of the respective years. This section lies within the subtropics and was the approximate latitude across which the GEOSECS program sampled eight stations. The model results will be compared with data in Section 7; here we present the transient as represented by the model.

In 1960 (Figure 3a) we see that the surface values are already highest in the eastern part of the basin. By 1970 (Figure 3b), when surface values in the eastern subtropics have reached their maximum values, the vertical gradient at 130°W is of order 200‰ over the upper 200 m. Although a significant zonal gradient exists in sea surface Δ^{14}C at this time, zonal gradients on constant depth horizons are small at depths >200 m. This remains true below 200 m depth through 1980, although the sea surface Δ^{14}C gradient decreases significantly between 1970 and 1980.

The corresponding Δ^{14}C distribution along 180°W is shown in Figure 4. During the 1960s the sea suface Δ^{14}C increase is largest between 20° and 45°N, which corresponds to the subtropics. By 1970, tongues representing subsurface maxima in Δ^{14}C can be seen to extend from the subtropics of both hemispheres toward the equatorial thermocline. In the mid 1970s the subsurface maximimum in the northern tongue exceeds 200‰, and the subsurface maximum in the southern tongue exceeds 100‰. However, as we shall see in the coral comparison, maxima of this order are never seen at the sea surface in the eastern equatorial Pacific in the 1980s. The model results along this section will also be compared with GEOSECS measurements in Section 7.

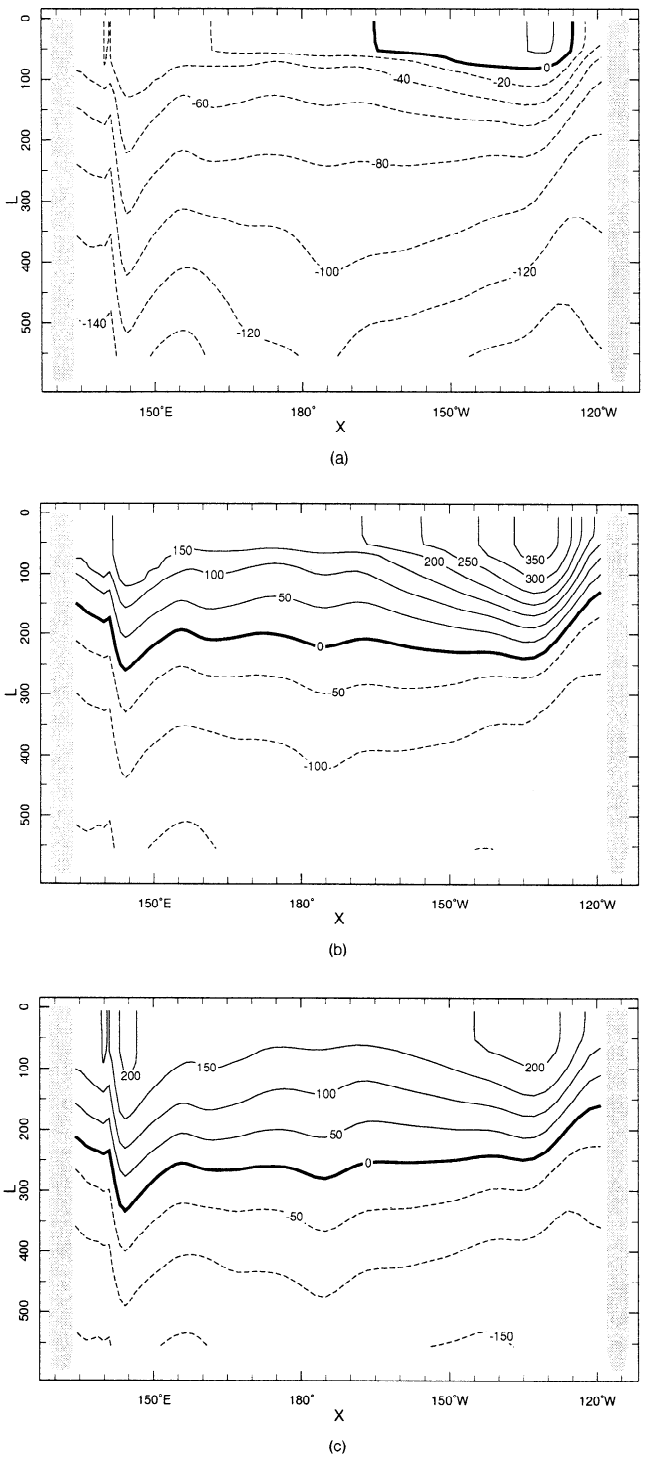

Figure 3. The evolving Δ^{14}C distribution along 32°N in (a) 1960, (b) 1970, and (c) 1980.

The plots shown in Figures 5a-5c show snapshots of the evolving distribution of Δ^{14}C on the σ_θ=25.0 surface. The shaded regions of the open ocean correspond to regions where the isopycnal surface has outcropped at the sea surface. These plots represent the Δ^{14}C distribution on January 1 of 1965, 1975, and 1985. The initial prebomb Δ^{14}C values in 1955 were uniformly low along the σ_θ=25.0 surface. By 1965 (Figure 5a), however, Δ^{14}C is present through much of the subtropical region, with maximum values in the Northern Hemisphere along the eastern part of the outcrop. The maximum values in the Southern Hemisphere stretch along the outcrop between 180° and 80°W. By 1975 the Δ^{14}C values on this surface have increased significantly, with maximum values in the eastern subtropics and minimum values in the upwelling regions. The zonal gra-

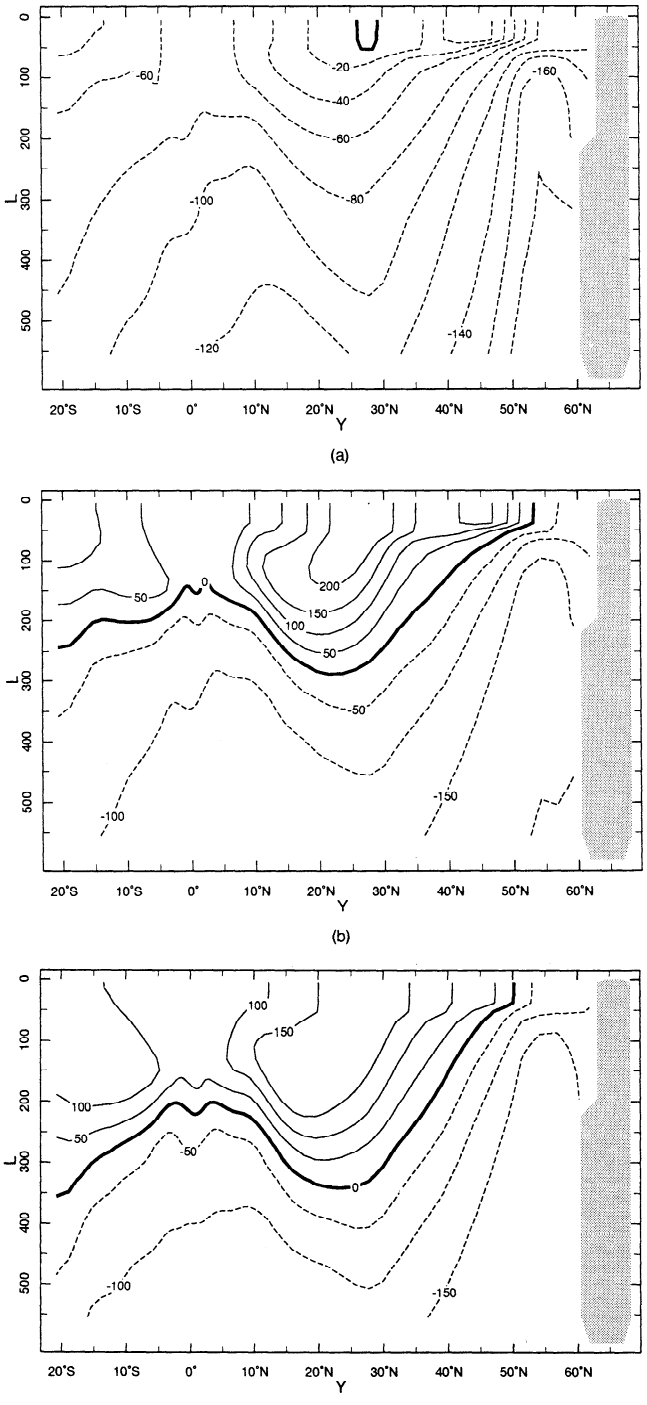

Figure 4. The evolving Δ^{14}C distribution along 180°W in (a) 1960, (b) 1970, and (c) 1980.

dient in Δ^{14}C in subtropical sea surface Δ^{14}C reflects the zonal gradient in sea surface conditions along the outcrop rather than zonal gradients in the ventilation rate within the subtropical thermocline.

By 1985 the subtropical values have diminished, which is expected given that atmospheric values had decreased monotonically since the 1960s (Figure 1). However, there is no great increase in equatorial Δ^{14}C values between 1975 and 1985 within 5° latitude of the equator, as one might expect from an idealized zonally averaged meridional cell with downwelling in the subtropics, upwelling in the tropics, and a ventilation time for the equatorial pycnocline of order 10 years.

It should be pointed out for the isopycnal surfaces shown in Figure 5 that some of the water that subducts

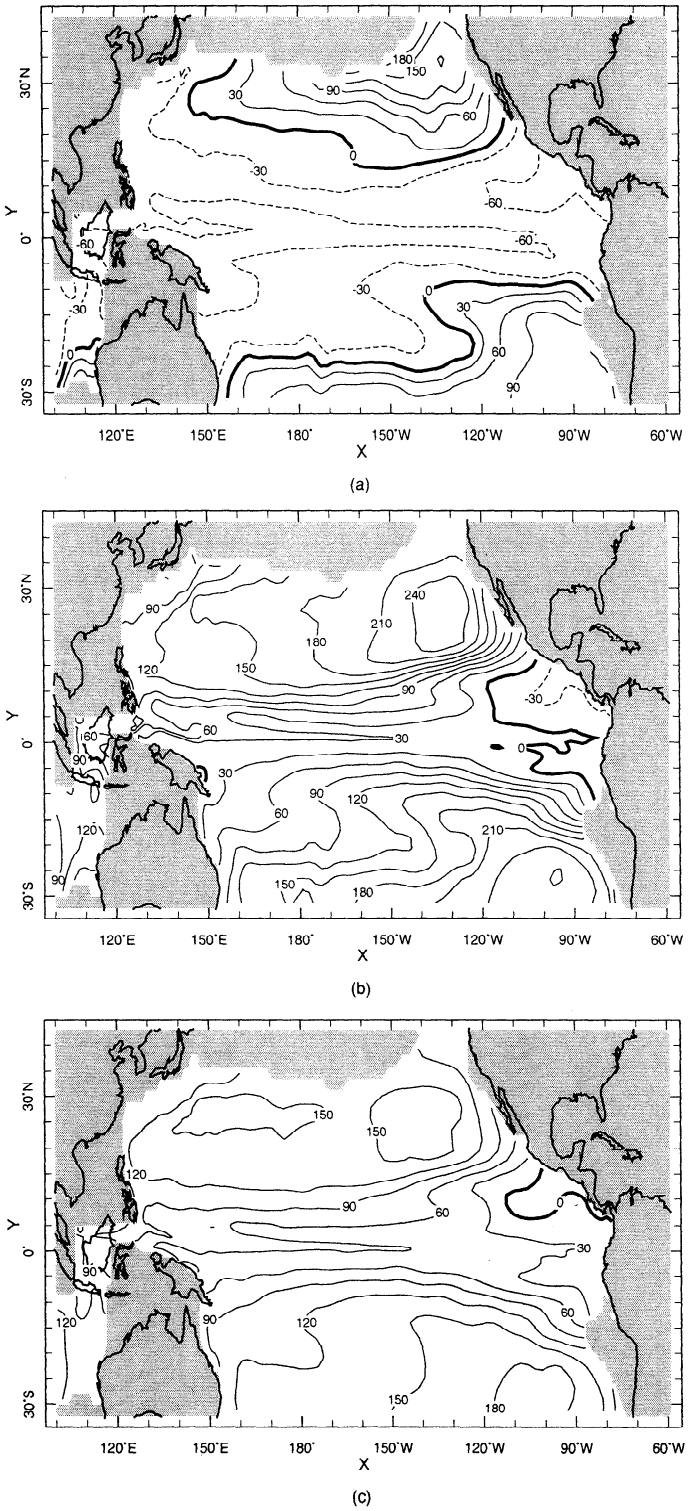

Figure 5. The Δ^{14}C distribution on the σ_θ=25.0 surface in 10 year increments for the control run (S10). The years shown are (a) 1965, (b) 1975, and (c) 1985.

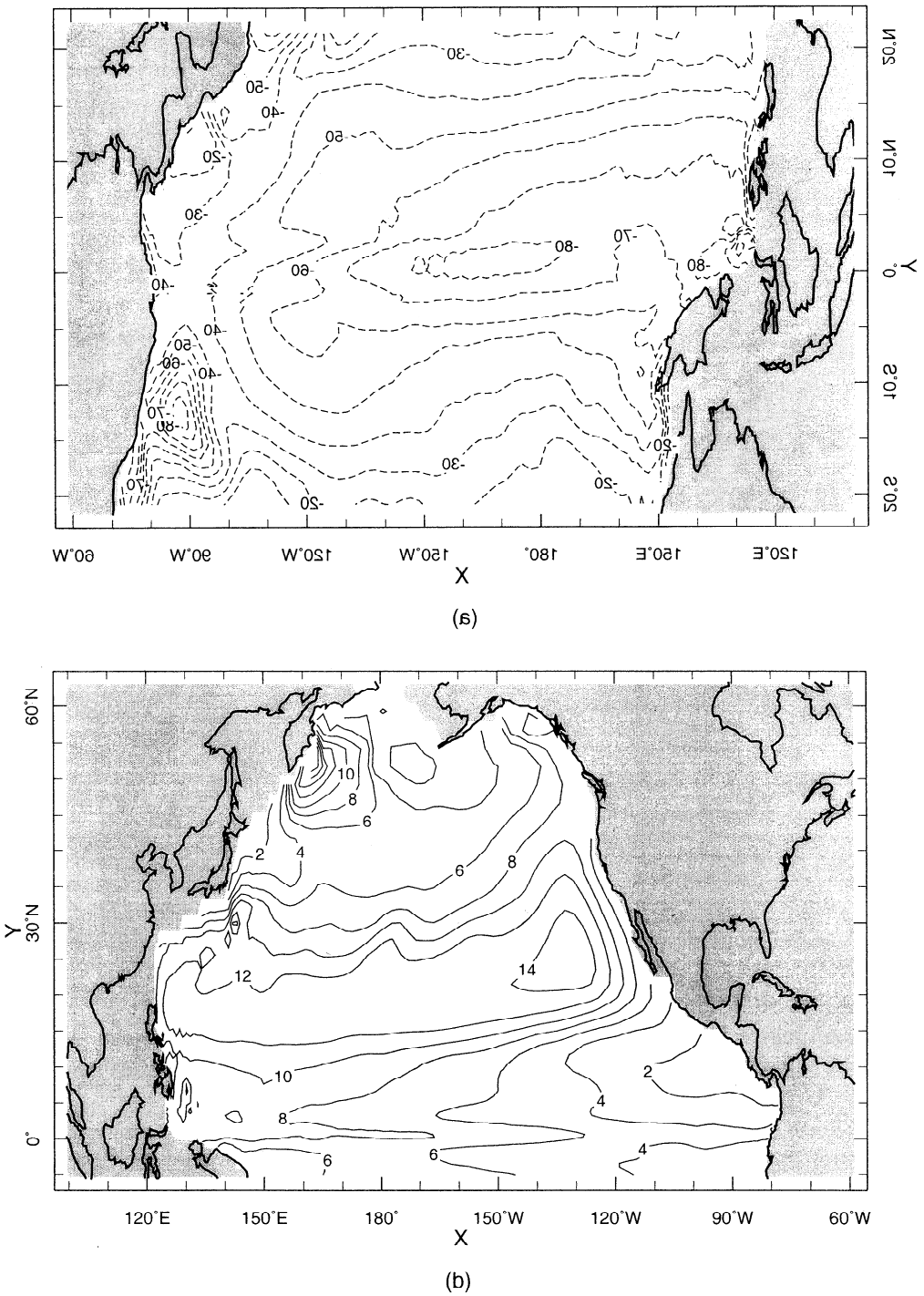

Figure 6. (a) Difference in sea surface Δ^{14}C between the S10 and S0 cases for the annual mean during 1974. Negative contours indicate lower Δ^{14}C values when the ITF transport is 10 as opposed to 0 Sv. The model inventories of bomb ^{14}C in units of 10^9 atoms cm^{-2} for January 1 1975 are shown for (b) the S0 case, (c) the S10 case, and (d) the S20 case.

in the subtropicical North Pacific recirculates within the subtropical gyre, while some advects toward the equatorial thermocline. The partitioning between these two ventilation pathways is largely dependent upon the longitude at which a water parcel subducts. Water subducting in the western part of the basin is more likely to undergo recirculation within the subtropics, whereas water that subducts to the east is more likely to experience intergyre exchange. The tongue of high-Δ^{14}C water seen along the equator on the σ_θ=25.0 surface in 1985 is tracing one of the important pathways of equatorial thermocline ventilation for S10, namely, subduction in the eastern subtropical North Pacific, advection to the western boundary via the North Equatorial Current, equatorward advection within the Mindanoa Current, and then eastward advection with the EUC.

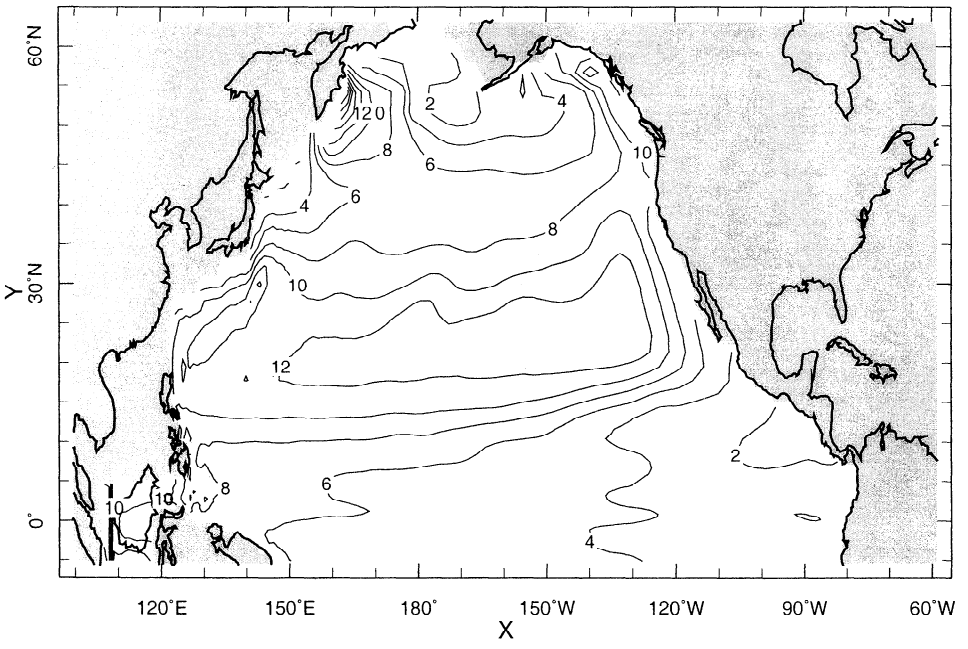

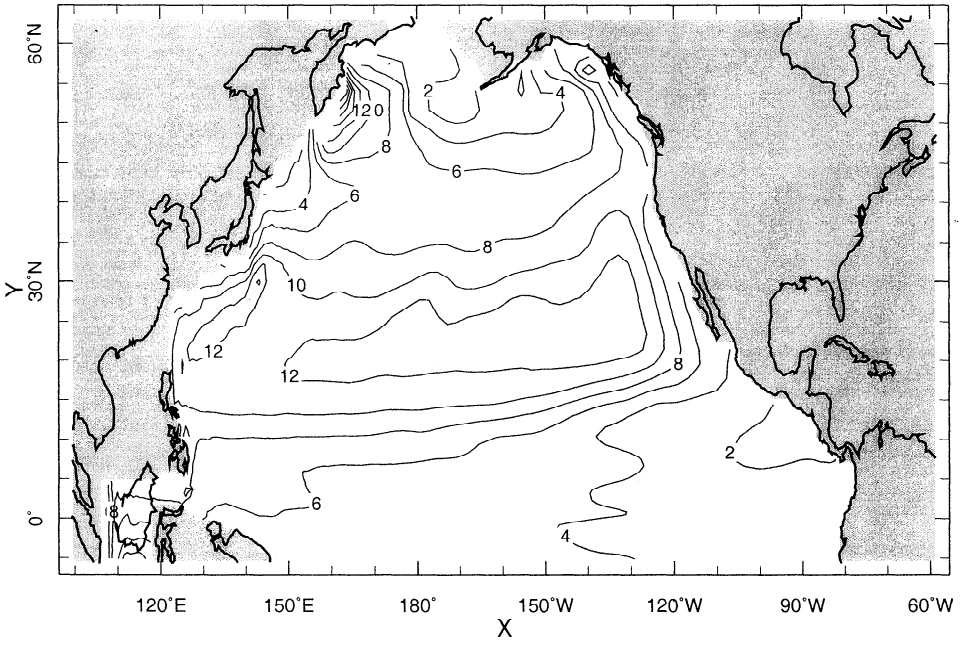

Figure 6. (continued)

Along the equator, in the western Pacific the approximate depth of this surface is 200 m. This advective pathway does not exist in course resolution models, as they do not capture the critical scales for the EUC.

6. Comparison of Cases With Different ITF Transports

The $\Delta^{14}C$ distribution calculated for the control case S10 has illustrated the pathways of model thermocline ventilation and intergyre exchange. Next we consider the way in which the treatment of the Indonesian Throughflow influences the bomb ^{14}C response of the equatorial Pacific.

Figure 6a shows the difference in annual mean sea surface $\Delta^{14}C$ between the S10 and S0 runs for 1974. Clearly, there is a significant offset in excess of 30‰ for most of the surface ocean between 20°N and 20°S, with a mean offset for this region of 55‰. There is a maximum difference located at ~160°W along the equa-

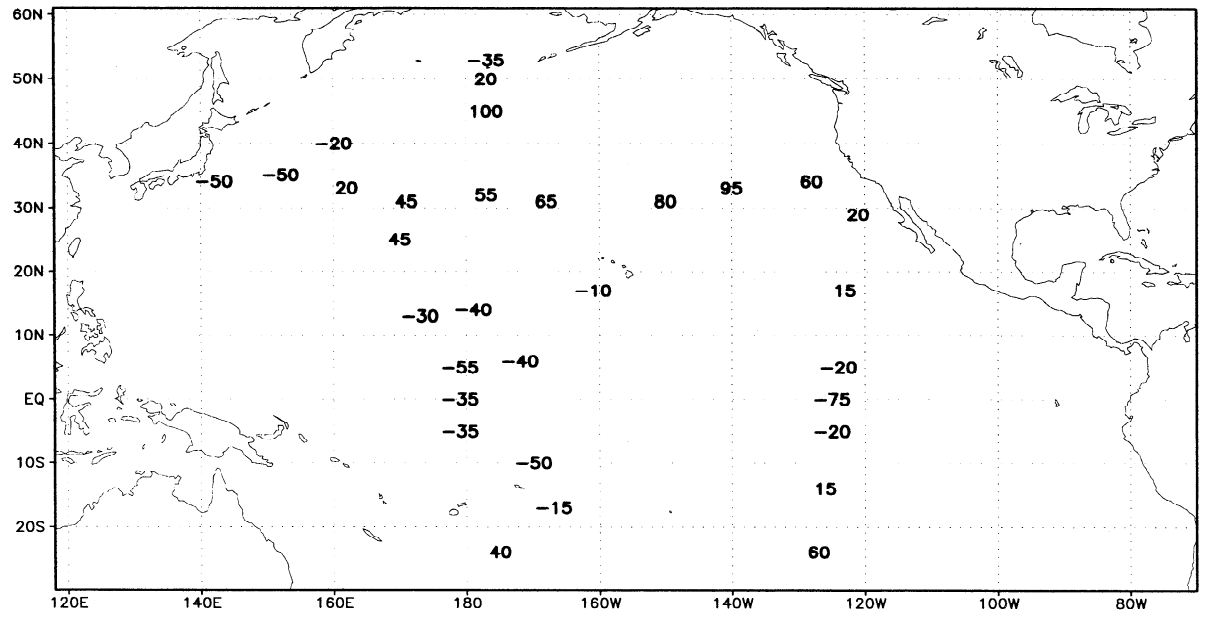

Figure 7. Geochemical Ocean Sections Study (GEOSECS) sea surface $\Delta^{14}C$; model minus data for S10.

tor. Case S0, which has no Indonesian Throughflow, is characterized by sea surface bomb $\Delta^{14}C$ levels, which are much higher than for S10. There is almost no difference in the sea surface $\Delta^{14}C$ distribution between the S10 and S20 runs for 1974.

Figures 6b, 6c, and 6d show the vertically integrated inventories of bomb ^{14}C for the S0, S10, and S20 cases on January 1 1975. The units for these plots are 10^9 atoms cm^{-2}. A comparison of the S10 case with data will be addressed in Section 7; for now we wish to point out the similarities and differences between the three cases.

The differences between the S0 and S10 cases are quite pronounced. Along the equator, inventories for the S0 case are more than 20% larger than for the S10 case. This is consistent with what we saw for the sea surface $\Delta^{14}C$ difference plot in Figure 6a. The inventories for the S0 case are also larger in the subtropics across 20°N than they are for the S10 case. Poleward of 30°N, the sign of the difference changes, with inventories for the S10 case being larger than for the S0 case. The sensitivity of the bomb ^{14}C inventories in the extratropical North Pacific to whether the ITF is open was certainly not an expected result of this study.

In comparison, the differences between the S10 and S20 cases are relatively insignificant. This is not only true of the depth-integrated inventories. The three-dimensional distribution of bomb^{14}C in the Pacific thermocline is nearly identical when examined on either depth levels or isopycnal horizons for the S10 and S20 cases. Although the thermocline $\Delta^{14}C$ distribution is quite sensitive to whether the ITF is open or not, it is nearly insensitive to whether the imposed tranport is 10 or 20 sverdrups.

7. Discussion

7.1. Data Comparison: Sea Surface $\Delta^{14}C$

Figure 7 shows the difference between the modeled $\Delta^{14}C$ distribution for the I15, case and the sea surface values measured during GEOSECS between August of 1973 and June of 1974. To account for the fact that the GEOSECS data were collected at different times, the model values at the location of each GEOSECS station were chosen to correspond to the particular month during which the station was sampled. This method of comparison allows us to avoid aliasing of seasonal and interannual variability in sea surface $\Delta^{14}C$.

Between 20° and 35°N the difference in sea surface $\Delta^{14}C$ increases from 20‰ at ~160°E, to 95‰ at 160°W. That the sea surface $\Delta^{14}C$ in the subtropics of the North Pacific is too large in the model is at least in part due to the fact that convective adjustment is not penetrating deep enough in this region during wintertime. The model overestimation of 95‰ at 160°W is approximately consistent with the overestimation obtained in the simulation of *Toggweiler et al.* [1989b]. For the two GEOSECS stations in the subtropical North Pacific closest to Japan between 140° and 155°E the sea surface $\Delta^{14}C$ in the model is less than the GEOSECS measurements. One possible explanation for this is that the model's horizontal resolution is still insufficient to resolve the western boundary currents in the subtropics.

The model's sea surface $\Delta^{14}C$ between 10°N and 10°S in the equatorial Pacific is less than the GEOSECS measurements. The point on the equator (125°W, 0°N) in the eastern Pacific where the model underestimates the GEOSECS measurement by 75‰ is perplexing. As was pointed out in an earlier process study [*Rodgers*

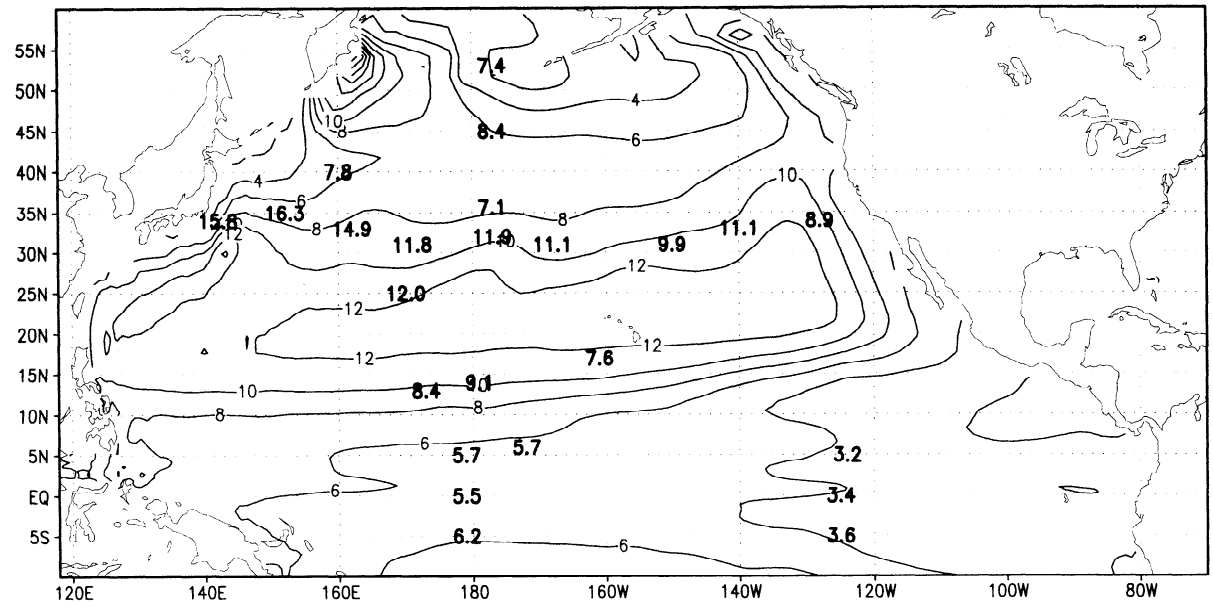

Figure 8. Model ^{14}C inventory for January 1, 1975 (case S10), with values inferred from GEOSECS measurements superposed. The units are 10^9 atoms cm^{-2}.

et al., 1997)], the sea surface GEOSECS $\Delta^{14}C$ value measured at the surface on the equator in the eastern Pacific is as high as the value measured on the equator in the western Pacific, whereas corals clearly indicate that a mean zonal gradient in sea surface $\Delta^{14}C$ existed across the equatorial Pacific in the 1970s. Whatever process in the real ocean acted to produce such an anomalously large $\Delta^{14}C$ value at this same point in May 1974 has not been captured by the model. As we shall see in Figure 8, the model adequately captures the depth-integrated inventory at 125°W, 0°N. As the discrepancy betweeen the model and the observations exists primarily for the surface $\Delta^{14}C$ value, we reiterate what we stated in our earlier study [*Rodgers et al.*, 1997], namely, that the sampling strategy of GEOSECS complicates model-data comparisons for particular grid points at particular times.

In the western equatorial Pacific, the model underestimates the sea surface GEOSECS $\Delta^{14}C$ measurements by 35-50‰. This is consistent with the offset that we will see between the Nauru coral time series at 165° and the model in a later section. One possible reason for this offset is that the gas exchange formulation underestimates the flux of ^{14}C from the atmosphere to the ocean in the warm pool region.

7.2. Data Comparison: Bomb ^{14}C Inventories and GEOSECS Data

A comparison of the model's bomb ^{14}C inventory for January 1, 1975, with the inventory calculated using Pacific GEOSECS measurements is shown in Figure 8. The inventories calculated from GEOSECS measurements [*Broecker et al.*, 1995] have been superposed on the model contours, and the units are 10^9 atoms cm^{-2}.

The GEOSECS survey intersected the equator at both 180° and 125°W in the Pacific Ocean. The data reveal a zonal gradient in the inventories across the equatorial Pacific of order 2 x 10^9 atoms cm^{-2}, and this is captured by the model. Of course, one must bear in mind that the vertical sampling density for the GEOSECS stations in the equatorial thermocline typically includes only four or five measurments in the upper 200 m, but nevertheless, the basin-scale features are captured by the model.

The spatial structure of the model inventory within the subtropical North Pacific is also in good agreement with the model. However, the comparison is complicated by the fact that the GEOSECS measurements tend to coincide with regions of large meridional gradients in the model. The tongue of maximum inventories across the central subtropical North Pacific appears to be shifted too far south in the model, although by how much is difficult to assess from the GEOSECS data.

Table 1. Summary of Bomb ^{14}C Simulation Runs

ITF Transport	Seasonal Forcing	Interannual Forcing
0 Sv	S0	
10 Sv	S10	
15 Sv		I15
20 Sv	S20	

For the case with seasonal winds, the seasonal climatology of *daSilva* [1994] is used. For the case with interannual winds the interannual climatology of daSilva is used to force the ocean model.

Table 2. Pacific Inventories for ^{14}C Atoms

Latitude Range	*Broecker et al.* [1985]	Lamont Model
40°-65°N	7.3	7.2
15°-40°N	35.9	32.9
10°S to 15°N	23.7	23.4
Total	66.9	63.5

Units are in 10^{26} ^{14}C atoms cm^{-2}.

A more thorough assessment of the model's simulated $\Delta^{14}C$ distribution in the subtropics will require a detailed comparison of the vertical structure of the simulated and observed $\Delta^{14}C$ distribution.

The integrated bomb ^{14}C inventories for the Pacific are represented in Table 2, where they are compared with the calculated budgets obtain from GEOSECS data [*Broecker et al.*, 1985]. The agreement between the model and the data is very good, especially considering that Broecker et al. estimate the error bars in their calculations to be of order 5-20%.

Next we consider the flux of bomb ^{14}C atoms from the Pacific to the Indian Ocean through the Indonesian Straits. In Table 3 the flux of bomb ^{14}C atoms from the Pacific to the Indian Ocean via the Indonesian Straits is tabulated as a function of time for the S10 run. The fluxes were calculated using the perturbation ^{14}C tracer. The first column of model output gives the flux for a particular year, and the second column gives the cumulative flux integrated from 1955 to the given year. Thus the model sends a flux of 9 x 10^{26} atoms to the Indian Ocean between 1955 and Pacific GEOSECS in 1974, which means that 1/8 of the bomb ^{14}C atoms delivered to the Pacific Ocean via gas exchange before the GEOSECS program were exported to the Indian Ocean via the ITF.

Table 3. Flux for Each Year and Cumulative Export of ^{14}C Atoms From the Pacific to the Indian Ocean Calculated Using the Perturbation ^{14}C Tracer

Year	Flux of ^{14}C Atoms	Cumulative ^{14}C Flux
1955	0.1	0.01
1956	0.3	0.04
1957	0.5	0.1
1958	0.7	0.2
1959	0.9	0.3
1960	1.4	0.4
1961	2.0	0.6
1962	2.6	0.8
1963	3.2	1.2
1964	3.9	1.6
1965	4.7	2.0
1966	5.6	2.6
1967	6.5	3.2
1968	7.5	4.0
1969	8.4	4.8
1970	9.1	5.7
1971	9.4	6.7
1972	9.7	7.6
1973	10.0	8.6
1974	10.3	9.7
1975	10.5	10.7
1976	10.4	11.8
1977	10.3	12.8
1978	10.2	13.8
1979	10.1	14.8

The units for the fluxes are 10^{25} atoms yr^{-1}, and for the cumulative fluxes are 10^{26} atoms

Table 4. Geochemical Ocean Sections Survey (GEOSECS) Indian Ocean Inventories, Estimated Local Input From Gas Exchange, and difference

Latitudes	Inventory	Gas Exchange Input	Deficit
25°N to 15°S	13.2	24.1	-10.9
15°S to 50°S	40.5	20.3	20.2

Units are 10^{26} atoms. This table is taken from *Broecker et al.* [1985].

By the time of Indian Ocean GEOSECS (early 1978), this accumulated flux of ^{14}C had increased to ~13 x 10^{26} atoms. The Indian Ocean GEOSECS data [*Broecker et al.*, 1985] are shown in Table 4, and comparing the model flux with the data tells us that ~25% of the total Indian Ocean inventory (53.7 x 10^{26} atoms) has come from the Pacific Ocean. In fact, our calculated flux from the Pacific to the Indian Ocean between 1955 and 1978 is nearly equal to the total inventory calculated by *Broecker et al.* [1985] between 15°S and the northern boundary of the Indian Ocean. Our model domain is able to tell us nothing about the eventual ventilation pathways of bomb ^{14}C-laden Pacific thermocline water upon entering the Indian Ocean. Suffice it to say that our results imply that the role of the ITF should not be ignored when considering Indian Ocean inventories of transient tracers.

7.3. Data Comparison: GEOSECS Sections

The model distribution of $\Delta^{14}C$ across 32°N on January 1, 1975, is shown in Figure 9a, with the observed GEOSECS values [*Ostlund and Stuiver*, 1980] along this transect superimposed. For the sake of comparison we shall consider $\Delta^{14}C$ to be a dye tracer, with the depth of the 0‰ isoline representing the penetration depth of the dye. Importantly, across the western and central regions of the subtropical North Pacific, the depth of the 0‰ isoline as recorded by the GEOSECS measurements has penetrated at least 50% deeper than the 0‰ line in the model. Of course, one should keep in mind that for this region the GEOSECS measurements occured ~1 year earlier than the model output field shown in Figure 9. However, this only helps to emphasize our point that the model is underestimat-

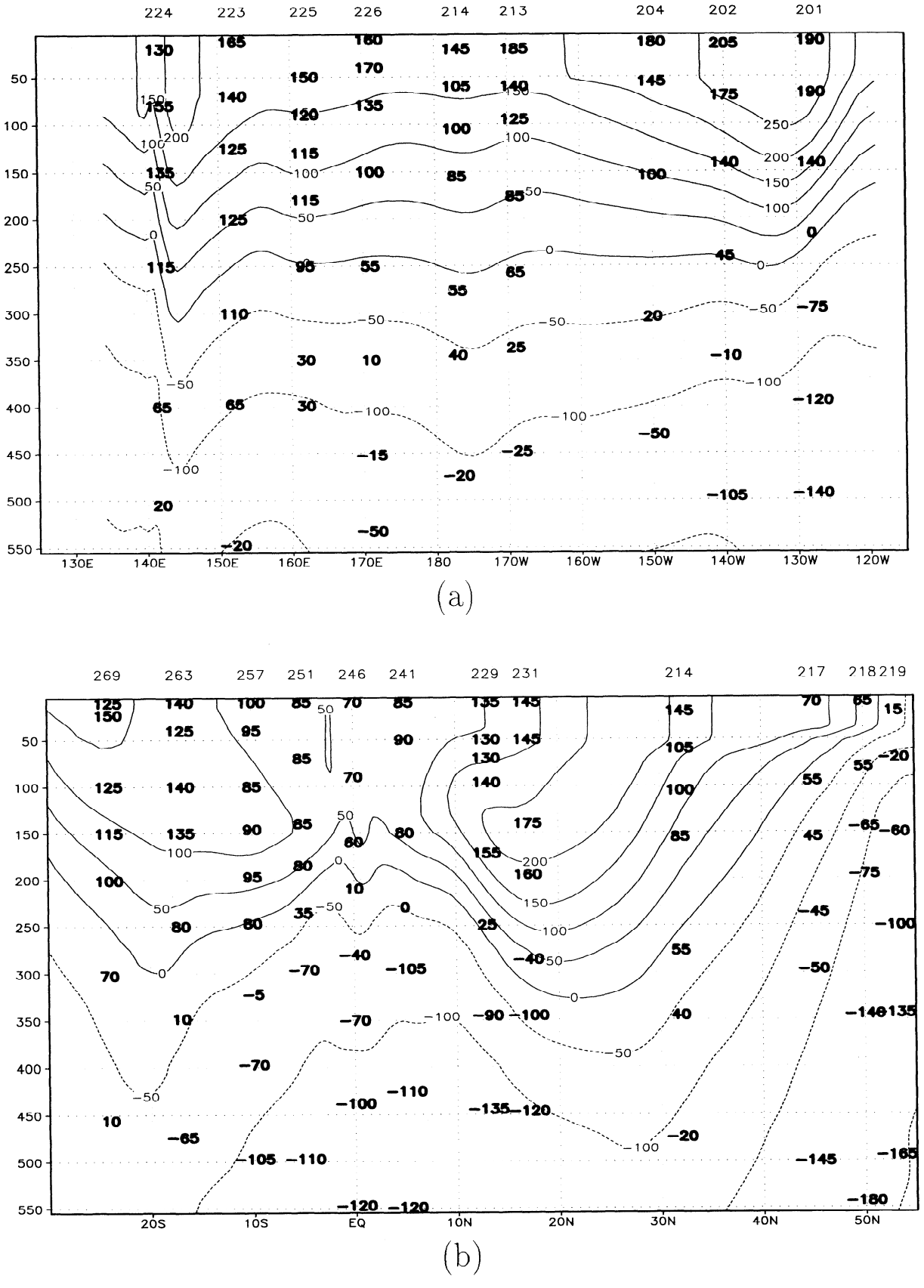

Figure 9. Δ^{14}C (a) as a function of longitude and depth across 32°N for the model in 1975, along with GEOSECS measurements, and (b) as a function of latitude and depth along 180°W. GEOSECS data are given in bold print, and GEOSECS station numbers are given across the top of the distributions. Also shown are (c) the simulated January temperatures across 32°N and (d) the Janaury values for the same section from the *Levitus and Boyer* [1994] monthly climatology.

ing the rate of ventilation of the western and central subtropical Pacific thermocline.

Given our interest in the penetration depth of transient tracers in the western Pacific and the observation in Figure 9a that the subtropical GEOSECS sampling of inventories coincides with regions of large gradients in the model, the question arises as to the validity of our claim with Figure 9a that the dye tracer is not penetrating to sufficient depth. This is addressed in Figure 9b, which shows the $\Delta^{14}C$ distribution according to the model on January 1, 1975, along 180°W. As can be seen with the GEOSECS data near 32°N, once again, the model $\Delta^{14}C$ is not penetrating to the same depth as that recorded by GEOSECS measurements anywhere within the subtropics along the dateline. In fact, this problem appears to be characteristic of both hemispheres along 180°W in our model simulation. As with the Northern Hemisphere, the penetration depth of the $\Delta^{14}C$ equals 0‰ isoline in the western part of the South Pacific subtropical gyre This is consistent with the findings of *Craig et al.* [1998], who simulated the distribution of CFC's in a global 1° version of the Geophysical Fluid Dynamics Laboratory (GFDL) Modular Ocean Model (MOM). In their study, the penetration depth of the 1 pmol kg^{-1} isoline for F11 is only half of what is seen in CFC data meausured between 1988 and 1990 along 170°W at both 35°N and 35°S. The same problem exists in their modeled F11 field at 165°E. Nevertheless, the F11 distribution in their equatorial pcynocline is in much better agreement with observations. Our results at 32°N are also consistent with the findings of the Ocean Model Intercomparison Project (OCMIP) program (J. Orr, personal communication, 1999), where the vertical structure of $\Delta^{14}C$ inventories in the North Pacific is underestimated for all of the ocean models compared in the project.

The extent to which the error in extratropical $\Delta^{14}C$ results from shortcomings in the model's representation of dynamical processes and the extent to which it represents problems in the parameterization used for gas exchange will be addressed in a future study. The modeled values in the surface waters of the eastern subtropics are larger than observations by ~100‰, as we saw in Figure 7 where we compared model results with GEOSECS data. This is largely due to the fact that the model is not adequately capturing the seasonal cycle in mixed layer depth for much of this region. Wintertime convection is seldom penetrating to as much as 50 m depth in the eastern subtropics, so that the upper ocean remains stratified through the year. The model's shallow wintertime convection at these latitudes is inconsistent with the data [*Huang and Qiu*, 1994], which shows a mixed layer depth in this region which is twice that of the model. This could be an artifact of the eddy mixing parameterization of *Gent and McWilliams* [1990], which when used in conjunction with high vertical resolution, is known to suppress convection [*Large et al.*, 1997].

Another factor contributing to the discrepancy between the model and observations in midlatitudes could be that our model has ~2.5° horizontal resolution in the extratropics. *Follows and Marshall* [1996] compared the bomb ^{14}C inventories in the North Atlantic for two different versions of the Community Modeling Effort (CME) model, one with 1° and one with 1/3° resolution. They found that eddy transfers in the 1/3° version of the model significantly enhanced the ventilation of the western subtropical gyre. In fact, the eddy-permitting experiment of Follows and Marshall is the only simulation of the bomb ^{14}C transient in the subtropics that has provided a satisfactory representation of tracer inventories in the western part of the subtropical thermocline. The *Gent and McWilliams* [1990] parameterization used in our study is intended to account for this effect, but it's clearly inadequate.

Despite the fact that the model is not adequately simulating the penetration of bomb ^{14}C into the lower thermocline of the western subtropical North Pacific, it is doing a reasonable job in maintaining the observed thermal stratification in this region. Figures 9c and 9d show the distrubtion of January temperature across 32°N, which is the same section shown in Figure 9a for $\Delta^{14}C$ for the model and data. For these distributions the simulated depths of the 12° and 14° isotherms are only 10% shallower than the values derived from the *Levitus and Boyer* [1994] monthly climatology for the same time. Thus the 50% disagreement between the model and data in the penetration depth of bomb ^{14}C for this region is not a reflection of problems in maintaining the stratification of the extratropical thermocline.

7.4. $\Delta^{14}C$ on Isopycnal Surfaces

The $\Delta^{14}C$ distribution on the σ_θ=25.0 surface for the S10 run is shown in Figure 10a. Vertically interpolated values from GEOSECS stations are superimposed on the model fields. Given the density of vertical sampling during GEOSECS, one must exercise caution in making detailed comparisons with the data. Thus, for the latitude belt between 20°S and 10°N the agreement between the model and the data is good since errors are less than 25‰. However, in the Northern Hemispheric subtropics the difference between the model $\Delta^{14}C$ distribution and the vertically interpolated GEOSECS data is >50‰, with larger differences in the eastern part of the gyre.

Figure 10b shows the model and GEOSECS data on the σ_θ=26.0 isopycnal surface. On this isopycnal surface the model is underestimating the $\Delta^{14}C$ levels in the Southern Hemisphere and overestimating the $\Delta^{14}C$ levels in the eastern part of the Northern Hemispheric subtropical gyre. In the western part of the subtropical gyre we see that the model is underestimating $\Delta^{14}C$.

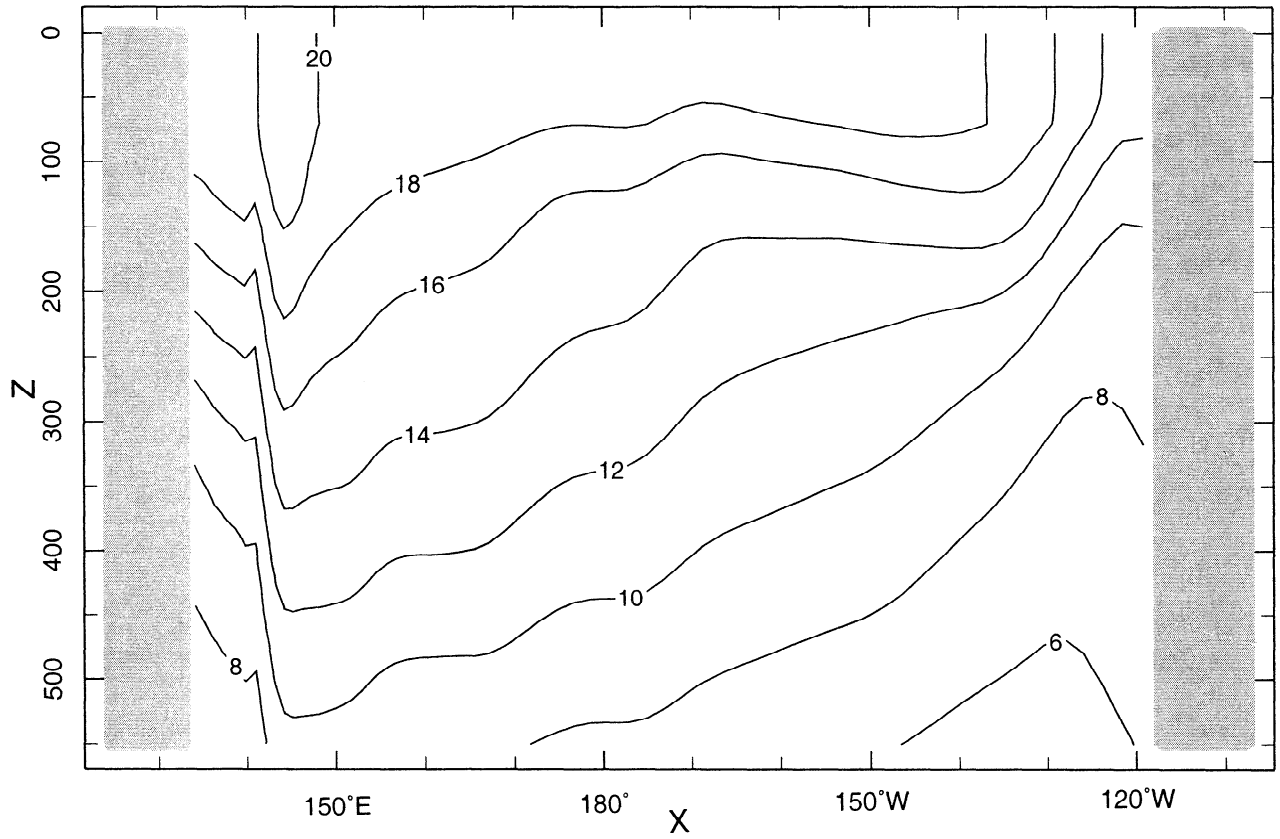

(c)

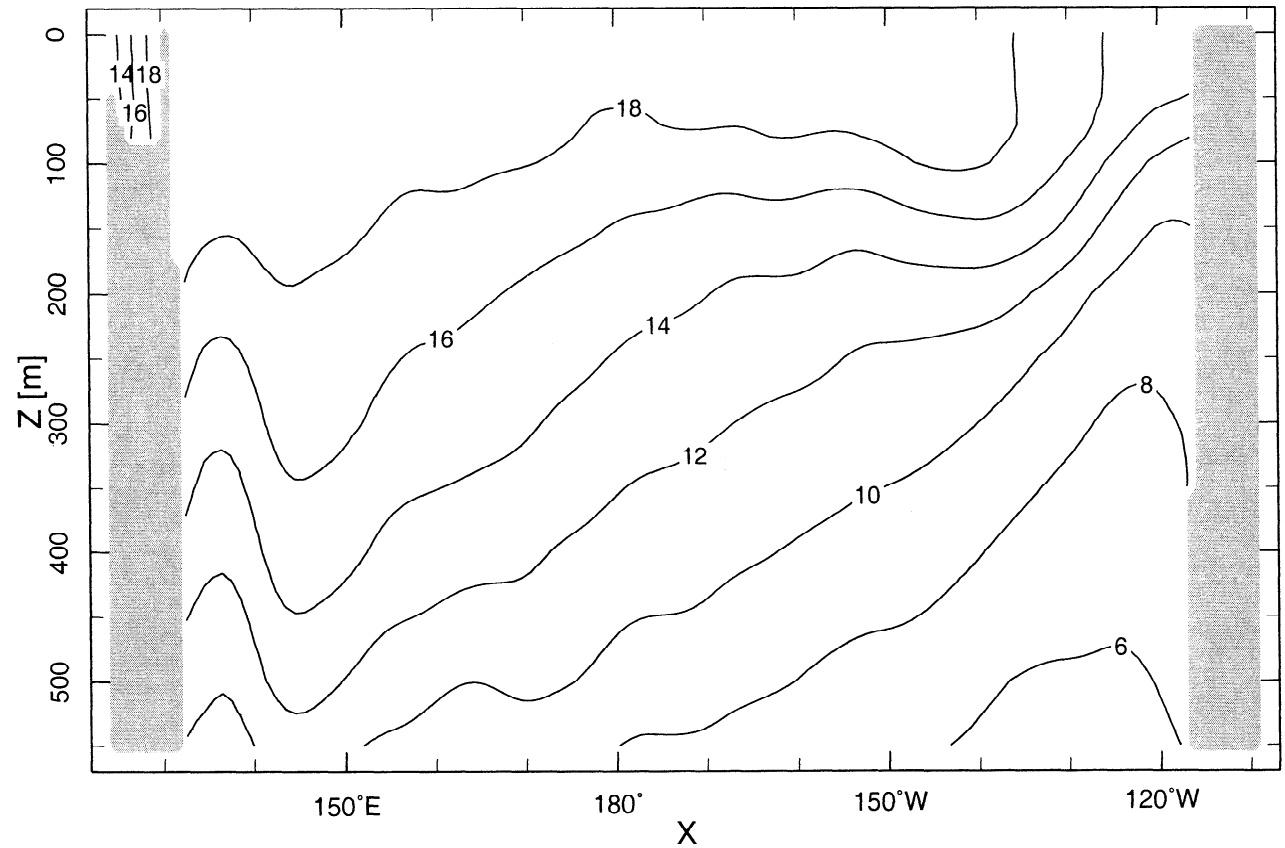

(d)

Figure 9. (continued)

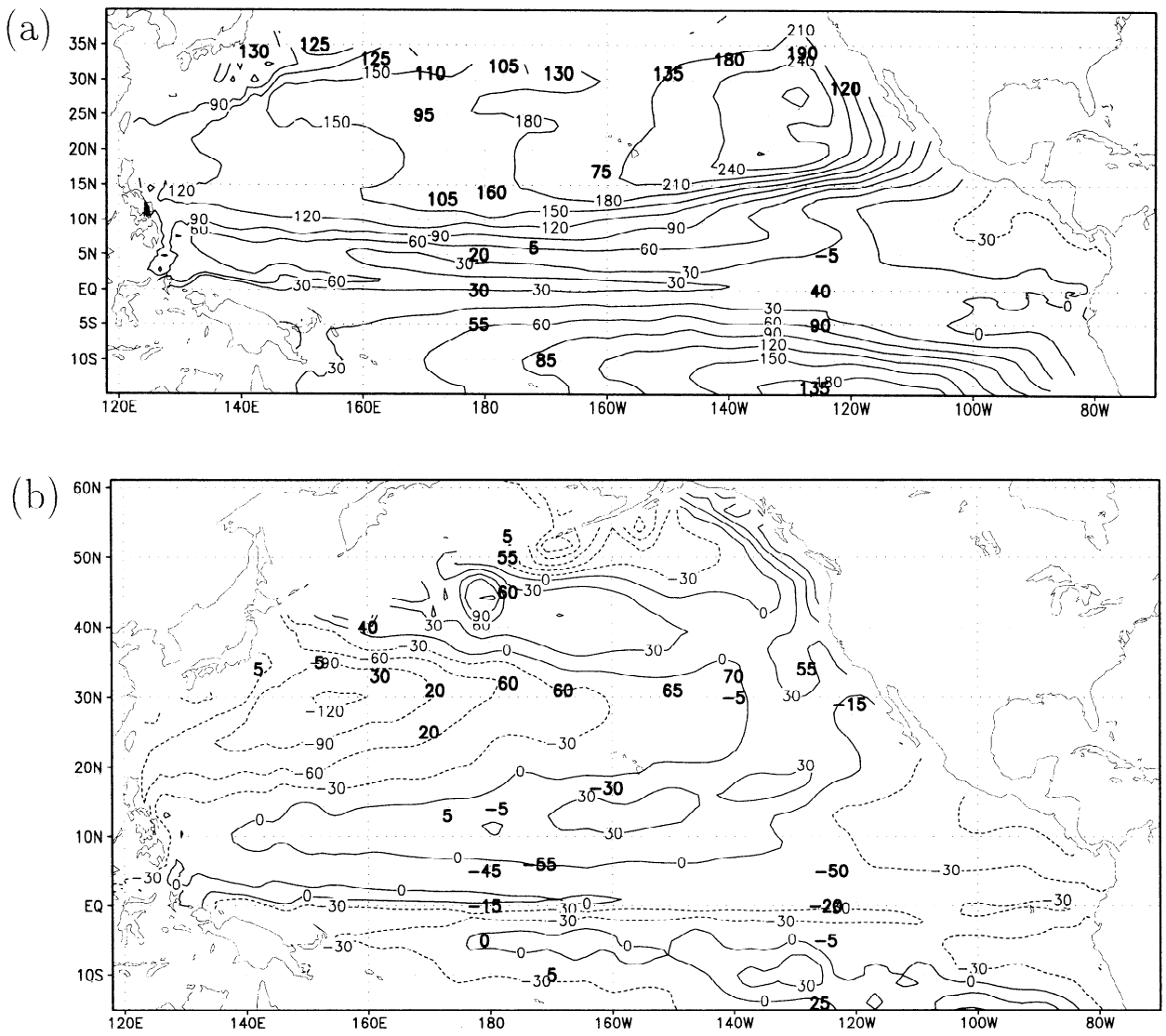

Figure 10. Δ^{14}C on January 1, 1975, for the S10 run on (a) the σ_θ=25.0 isopycnal surface and (b) the σ_θ=26.0 isopycnal surface. GEOSECS data are given in bold print.

which is the same problem we saw at depth in the western subtropics in Figure 9a.

7.5. Penetration Depth of Δ^{14}C Isolines

The depth of the Δ^{14}C=0 isosurface on Januray 1, 1975, is shown in Figure 11, with GEOSECS data superposed. Consistent with what we have seen before, the model is significantly underestimating the penetration depth of the bomb ^{14}C signal in the western subtropical North Pacific. The simulated penetration depth in the eastern subtropical North Pacific, on the other hand, is in much better agreement with the GEOSECS measurements. The penetration depth of the Δ^{14}C=0 isosurface in the tropics is also in reasonably good agreement with the data.

To demonstrate that our conclusion was not biased by the arbitrary choice of the Δ^{14}C=0 isosurface, this comparison was repeated again for both the Δ^{14}C=-25 and -50‰ isosurfaces. The results on these surfaces are the same: namely, the model significantly underestimates the depth of the isosurface in the wetsern subtropics of the Northern Hemisphere but compares reasonably with data in the eastern subtropics and within the equatorial thermocline.

7.6. Data Comparison: North Pacific Experiment

The Pacific component of the global GEOSECS survey represented the first synoptic survey of Δ^{14}C in the Pacific Ocean. However, the vertical sampling density within the equatorial thermocline during GEOSECS typically included only four samples in the upper 200 m. It was not until the North Pacific Experiment (NORPAX) survey [*Quay et al.*, 1983] along 150° and 160°W during 1979 and 1980 that the equatorial thermocline was sampled with sufficient density to resolve the vertical structure of Δ^{14}C in the equatorial pycnocline.

The meridional section plots of Δ^{14}C in the equato-

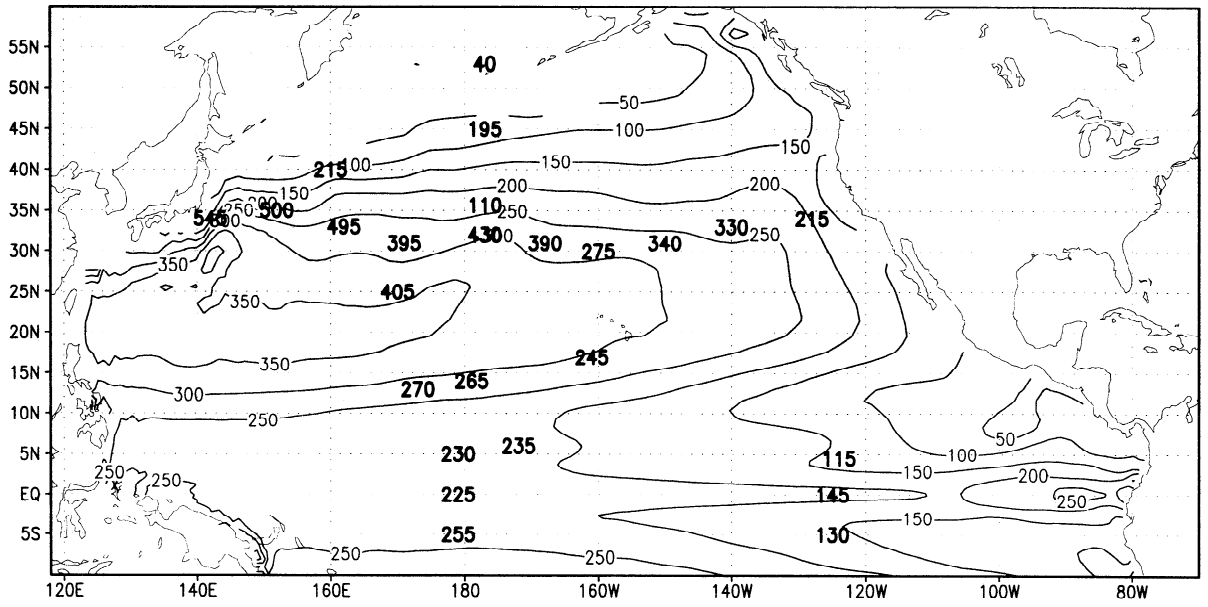

Figure 11. The depth of the $\Delta^{14}C$=0 isosurface on January 1, 1975, for the S10 run. GEOSECS data are given in bold print.

rial thermocline from the study of *Quay et al.* [1983] are shown in Figure 12. Figure 12a shows the distribution as a function of latitude and depth, and Figure 12b shows the distribution as a function of latitude and density. The $\Delta^{14}C$ distribution measured along this transect is relatively symmetric about the equator. It is clear for the latitude versus density plot that the maximum subsurface $\Delta^{14}C$ signal on the density range surrounding σ_θ=25.0 does not extend to the equator, but rather forms a subsurface tongue which extends in from the subtropics. Nevertheless, the $\Delta^{14}C$ values on the equator on the σ_θ=25.0 density horizon are well above their prebomb levels of ~-70‰.

Some interhemispheric differences in the $\Delta^{14}C$ distribution along 150°W warrant mention. The distribution is characterized by a subsurface maximum in $\Delta^{14}C$ for the Northern Hemisphere that is centered between the σ_θ=24.5 and 25.0 isopycnal layers. According to the March sea surface temperatures and salinities [*Levitus and Boyer*, 1994], this corresponds to a March outcrop between 25° and 30°N. For the Southern Hemisphere the maximum $\Delta^{14}C$ is centered between the σ_θ=25.0 and 25.5 density layers. This corresponds to a Southern Hemispheric winter outcrop between 30°S and 35°S.

The model results shown in Figure 12c represent a snapshot of model conditions for January 1, 1980, for the S10 case. The model reproduces the major features of the data, namely the subsurface tongues of high $\Delta^{14}C$ extending from the surface waters of the subtropics in either hemisphere into the equatorial thermocline, and it captures these tongues at the correct depth level. The asymmetry about the equator in the maximum subsurface $\Delta^{14}C$ values is also captured by the model, with larger values to the north and smaller values to the south.

7.7. Data Comparison: Coral Time Series

Next we compare the model results with existing coral $\Delta^{14}C$ data from the Pacific Ocean. Time series for four sites are shown in Figure 13: French Frigate (23°N, 166°W), Galapagos (1°S, 90°W), Fiji (18°S, 179°E), and Nauru (1°S, 167°E). French Frigate lies in the subtropics of the Northern Hemisphere, Fiji in the subtropics of the Southern Hemisphere, Galapagos in the eastern tropics, and Nauru in the western tropics. For each site we show the model output for the I15 run (black) and the coral data (shaded).

First we consider French Frigate (Figure 13a). The coral data [*Druffel*, 1987] represents annual mean values. The coral data peak at 180‰ in the early 1970s. The model simulation peaks a few years earlier, and the maximum offset between the model and the data is 50‰ in 1968. By the time of Pacific GEOSECS the offset between the model and the data is quite small.

Next we consider the model's simulation of the bomb transient at Galapagos (Figure 13b). The coral $\Delta^{14}C$ data set shown is that of *Guilderson and Schrag* [1998]. In contrast to French Frigate, the $\Delta^{14}C$ values at Galapagos exhibit a gradual increase through the 1970s. The agreement between the simulation and the observations is quite good, although the model slightly overestimates sea surface $\Delta^{14}C$ in the late 1960s and slightly underestimates the values for the late 1970s and early 1980s. *Guilderson and Schrag* [1998] have pointed out that seasonally minumum coral $\Delta^{14}C$ is characterized by an abrupt jump in 1976. This is not reproduced by the model, which shows a gradual increase in its seasonally minimum $\Delta^{14}C$ through the 1970s.

Next we consider the Fiji site (Figure 13c). Here the coral data [*Toggweiler*, 1983] are seen to be in good

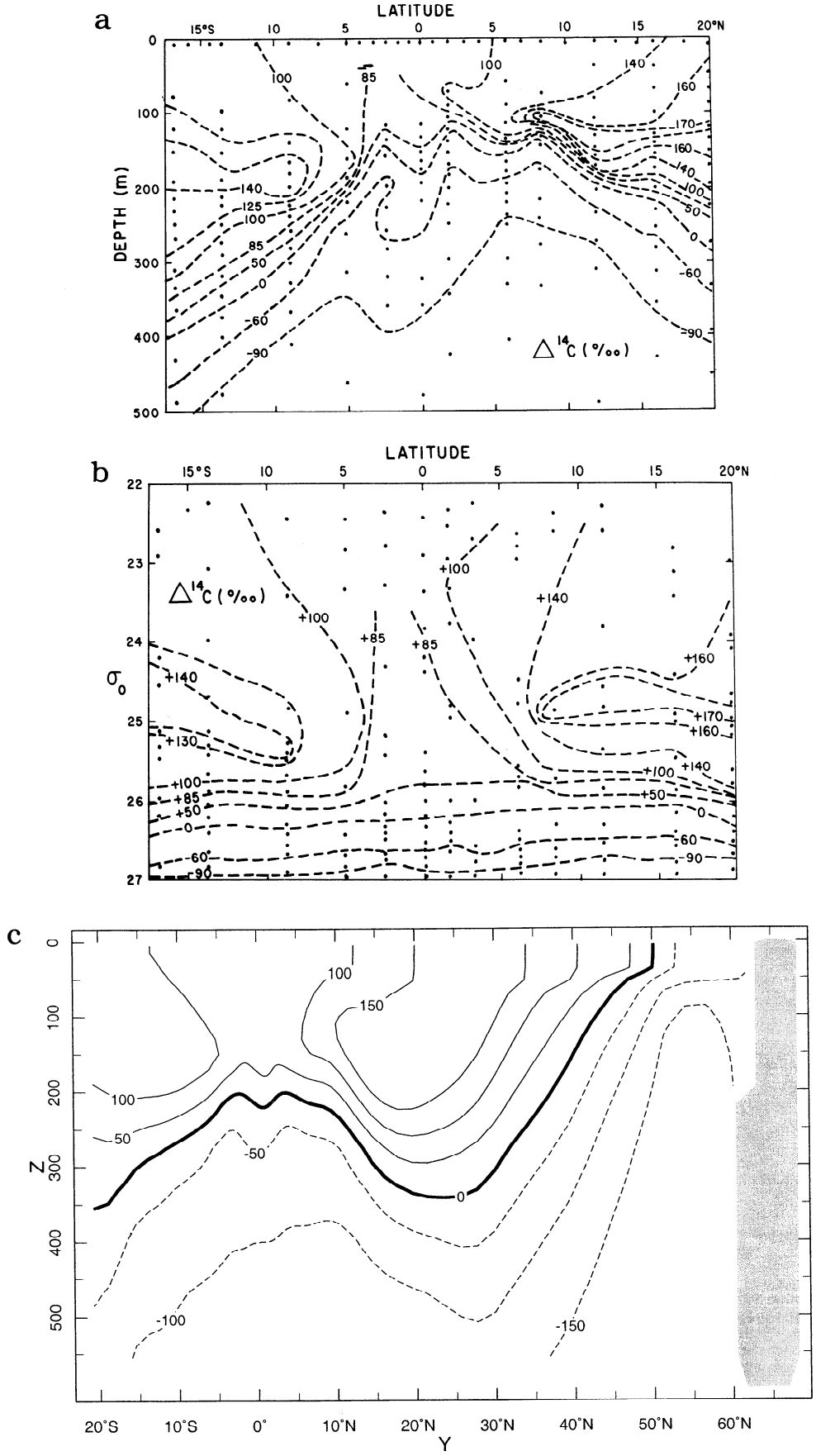

Figure 12. (a) The $\Delta^{14}C$ along 150°W measured in 1979 during the Hawaii to Tahiti Shuttle as a funtion of latitude and depth [*Quay et al.*, 1983]. (b) The same quantity plotted as a function of latitude and potential density. (c) The model's $\Delta^{14}C$ at 150°W as a function of latitude and depth on January 1, 1980.

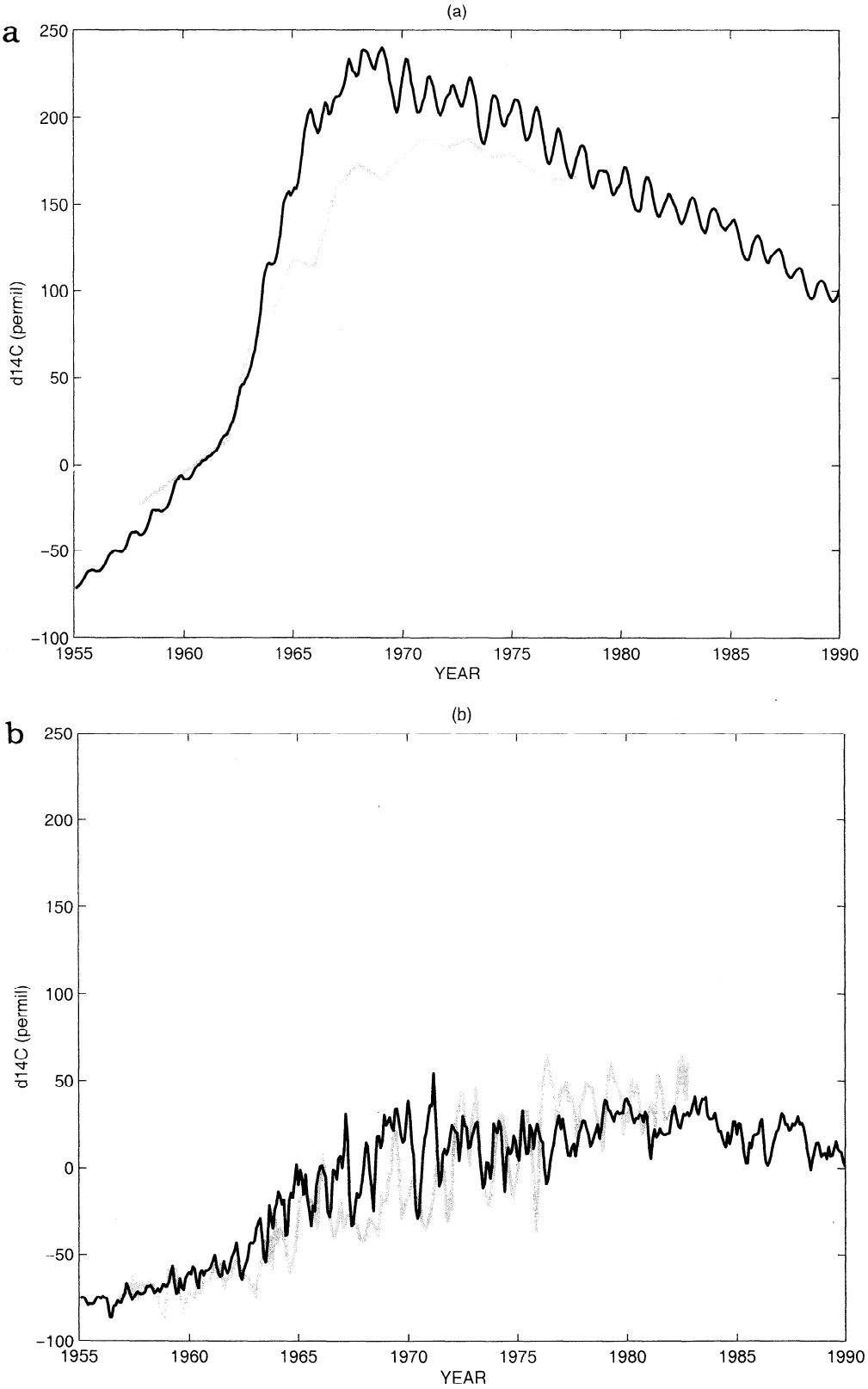

Figure 13. Model (black) and coral (shaded) Δ^{14}C for (a) French Frigate, (b) Galapagos, (c) Fiji, and (d) Nauru.

agreement with the model simulation. As with the French Frigate coral, this subtropical site peaks in the early 1970s before declining through the 1980s.

Finally, we consider the Δ^{14}C signal for Nauru Island (Figure 13d). The coral curve is from the high-resolution data of *Guilderson et al.* [1998]. The offset between the model and the data is ~40‰ through the 1970s. This offset is consistent with the offset measured at 180°W during GEOSECS [*Ostlund and Stuiver*, 1980]. In particular, the model captures the spike

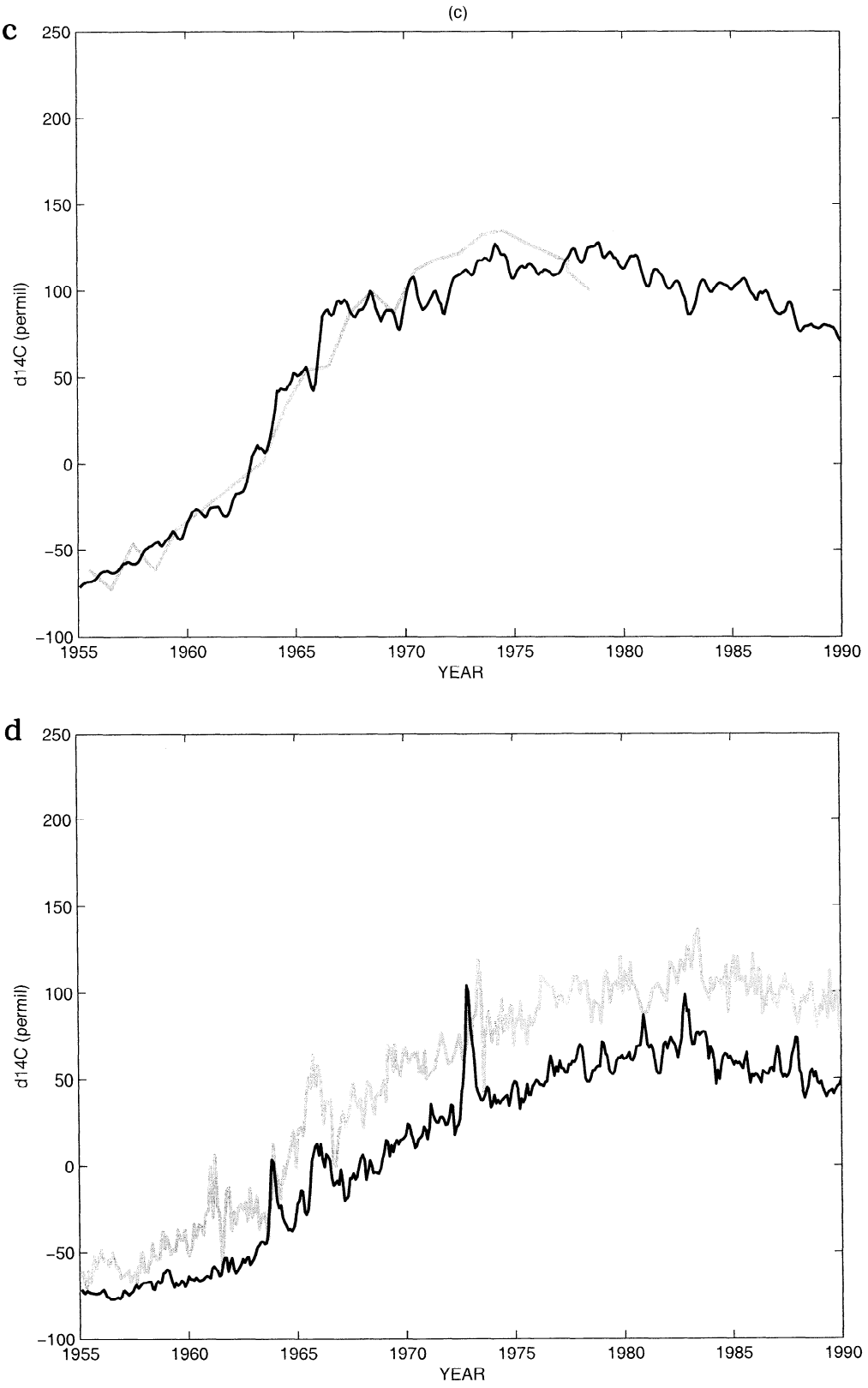

Figure 13. (continued)

associated with the 1972-1973 El Niño, although the peak in the model occurs some 5 months earlier than the peak in the data. In the model the spike is caused by an eastward surge of surface waters with high Δ^{14}C from the Mindanao Current to the east along the equator.

There are several possible reasons why the model's Δ^{14}C along the equator during the early 1970s could be lower than the values measured during GEOSECS and the values recorded by equatorial corals. One possibility is that the gas exchange formulation used for this study is inadequate. This is quite likely at Nauru since

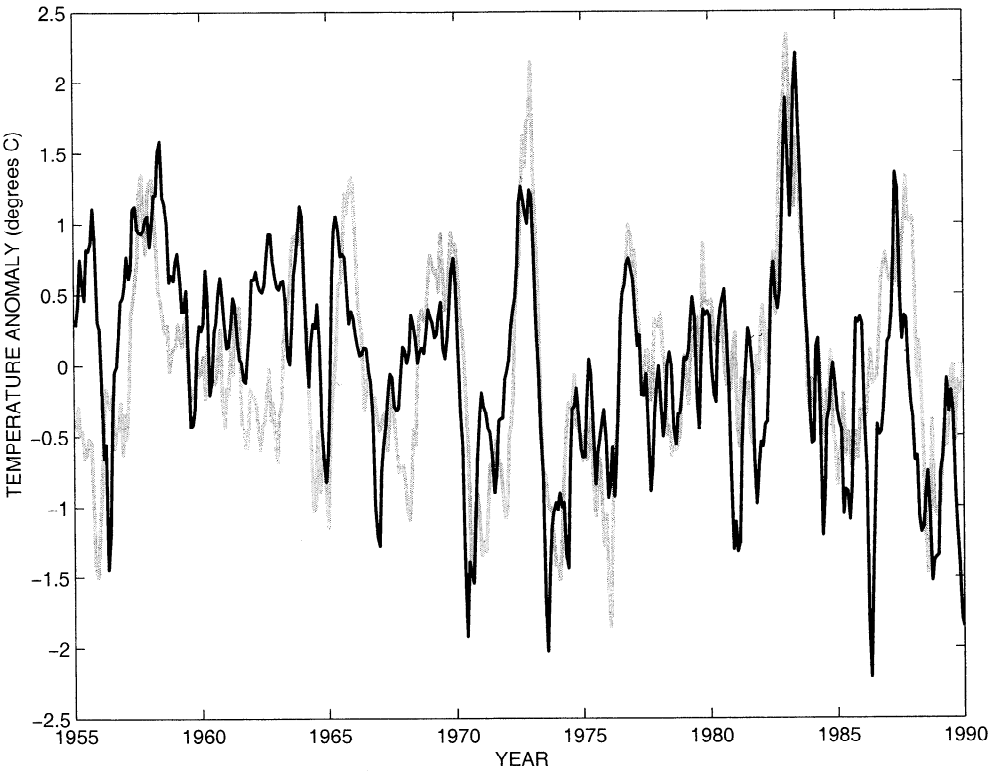

Figure 14. Comparison of modeled (black) and observed (shaded) [*Kaplan et al.*, 1998] NINO3 SST anomalies between 1955 and 1990.

the wind speeds over the warm pool in the ECMWF climatology are not very large. However, local tropical wind speeds should not be so important at Galapagos since the supply of bomb ^{14}C via intergyre exchange should be more important.

A second possible explanation is that by imposing a fixed ITF transport for these runs we have compromised the mean Δ^{14}C of the surface waters for the equatorial Pacific. We have seen that for the S0 case the mean sea surface Δ^{14}C for the equatorial Pacific is significantly larger than for the other cases. In fact, the sea surface Δ^{14}C distribution for the S0 case is in better agreement with the GEOSECS data than the others. However, we rule this possibility out by the argument that when the ITF is closed, the mixing ratio of northern to southern component waters in the equatorial thermocline is distorted [*Rodgers et al.*, 1999].

A third explanation for the model's equatorial sea surface Δ^{14}C being somewhat lower than the GEOSECS measurements is that the model is too diffusive. We have seen in our comparison of the Δ^{14}C distribution measured in the equatorial thermocline during NORPAX (Figure 12a) and the Δ^{14}C for the model for January 1, 1980, at the same location (Figure 12c) that if anything, the model overestimates the Δ^{14}C at 10°N and 10°S. This points to the low-latitude western boundary currents (LLWBCs) and the EUC as potential locations of spuriously large diapycnal diffusivity in the model, which would have the effect of entraining deeper waters and diluting the Δ^{14}C signal. It is most likely that excessive mixing within the equatorial undercurrent is diluting the sea surface Δ^{14}C signal in the equatorial Pacific in the early 1970s.

A comparison of the SST anomalies in the eastern equatorial Pacific for the I15 case and the dataset of *Kaplan et al.* [1998] is shown in Figure 14. For both cases, temperature anomalies are calculated over the NINO3 region, i.e., over a box ranging in latitude from 5°S to 5°N and from 90° to 150°W in longitude.

It should be kept in mind that wind stress data for the equatorial Pacific is quite sparse before the 1970s, so that the model's interannual variability in sea surface temperature during this period should not be expected to match observations. In addition, for the I15 case we forced the model with interannually varying winds, but heat fluxes were calculated using seasonally varying climatologies. Given these limitations, the match between the model and the data for this region is quite satisfactory. It is interesting to note, however, that although the model represents a shift in SST in 1976, it fails to do so with Δ^{14}C, as was seen in Figure 13b.

7.8. The Subtropical Cell and Intergyre Exchange

It was mentioned earlier that the evolution of the bomb Δ^{14}C transient in the Pacific thermocline has a bearing on climate questions. For the zonally averaged circulation in the Pacific a meridional subtropical cell

(STC) exists in the surface and thermocline waters. The surface water that subducts in the eastern part of the subtropical gyres moves equatorward within the thermocline and, upon upwelling along the equator some 10-20 years later, returns to the midlatitudes via the surface Ekman flow. *Wyrtki* [1981] used mass, heat, and salinity budgets to argue that the strength of the equatorial upwelling is ~50 Sv. Assuming that only 5 Sv of this represents local recycling of equatorial water implies that the strength of the STC is 45 Sv.

The northern boundary of the STC coincides with the zero wind stress curl line separating the subpolar and subtropical gyres of the North Pacific, or approximately the outcrop of the σ_θ=26.2 isopycnal, and the southern boundary corresponds to the outcrop of the same isopycnal. The σ_θ=26.2 will define the lower boundary of our STC as it delimits the lower bound of the directly ventilated thermocline [*Huang and Qiu*, 1994], with the upper boundary being the sea surface.

That this cell is not closed can be seen by considering a simple budget calculation involving the Indonesian Throughflow. The ITF represents a mean flux of thermocline water out of the Pacific basin, and given that the estimates of ITF transport are in the range 5-16 Sv [*Godfrey*, 1996], this constitutes a flux that is equivalent to 10-35% of the strength of the STC. The mass flux associated with the ITF outflow must be balanced in steady state by an entrainment of colder water into the STC.

Toggweiler et al. [1991] have used measurements of prebomb Δ^{14}C to argue that there is significant entrainment of deeper water into the STC. One important difference between our analysis and that of Toggweiler et al. lies in the source of the low prebomb Δ^{14}C water recorded by Galapagos corals. Toggweiler et al. argued that the 13° thermostad water that lies below the equatorial undercurrent [*Tsuchiya*, 1981] upwells off the coast of Peru and then advects over Galapagos within the South Equatorial Current. However, for the high resolution model used in our study the surface water surrounding Galapagos is supplied alternatively by the EUC and the southward advection of a Δ^{14}C front lying just to the north of the equator through the seasonal cycle. The water that upwells off Peru is advected poleward within the surface Ekman flow in the Southern Hemisphere. Thus, whereas Toggweiler et al. looked to the Peru Upwelling as the source of low prebomb Δ^{14}C recorded by Galapagos corals, our model implicates thermocline water within the EUC.

There are two important pathways by which low-Δ^{14}C waters could be entrained into the STC. The first of these is via diapycnal fluxes within the thermocline. Diapycnal fluxes cause colder water from deep thermocline to intermediate depths to mix with water in the pycnocline. The plot shown for the Δ^{14}C as a function of latitude and potential density anomaly at 150°W in 1979 (Figure 12b) suggests that significant dilution is occuring in the latitude belt of the equatorial current system, since the subsurface maxima in Δ^{14}C do not manage to ever reach the EUC. A quantification of this entrainment will be important for understanding thermal budgets.

A second pathway by which low-Δ^{14}C water can become entrained into the STC is via Ekman flow at the ocean surface. A sizeable fraction of the water that subducts in the subtropical convergence of both hemispheres of the Pacific Ocean is supplied by the equatorward Ekman flow from the subpolar gyre of the North Pacific and from the Antarctic Circumpolar Current (ACC) region of the Southern Hemisphere. That this water maintains its low-Δ^{14}C signature upon subducting in the subtropics is due to the decadal air-sea equilibration timescales for carbon isotopes, whereas its temperatures and salinity properties are significantly modified through heat and freshwater fluxes. A quantification of the effect of this process, which involves intergyre exchange between the subtropical and subpolar regimes, on Δ^{14}C inventories in the STC will be addressed in a future study.

Enhanced equatorial resolution in ocean models is also important in simulations of the oceanic carbon cycle. *Aumont et al.* [1999] have shown that when meridional resolution of 0.5° is used in the vicinity of the equator, the extent of nutrient trapping is greatly reduced.

8. Conclusions

The bomb ^{14}C transient for the Pacific Ocean has been simulated using a high-resolution primitive equation ocean circulation model. The control run, which was forced with seasonally varying winds and buoyancy fluxes, reproduces the observed large-scale features of the bomb Δ^{14}C transient in the Pacific thermocline. Sea surface Δ^{14}C peaked within the subtropics of the Pacific Ocean in the late 1960s and early 1970s but continued to rise in the equatorial Pacific through the 1970s and into the 1980s. The lag in the rise of tropical sea surface Δ^{14}C with respect to the subtropics is controlled by the advective timescale for intergyre exchange of thermocline water between the subtropics and the tropics of the Pacific Ocean.

The model's basin-wide bomb^{14}C inventories for the Pacific Ocean are in very good agreement with the inventories calculated from GEOSECS measurements. In particular, the model inventories in the equatorial Pacific are consistent with the data in absolute magnitude, and the model captures the zonal gradient in the inventory between 125° and 180°W. We attribute this success to the high meridional resolution for the equatorial Pacific used in our study, which allows us to resolve the critical scales of equatorial circulation.

This study was motivated by our interest in intergyre exchange as an oceanographic process with important implications for climate variability. The same mixing and advective processes that control the intergyre ex-

change of $\Delta^{14}C$ also impacts the propagation of thermal anomalies within the ocean. The model results for the control run are generally consistent with the $\Delta^{14}C$ measurements collected during the GEOSECS and NORPAX surveys. The most important difference between the model and the GEOSECS is reflected in the fact that the simulated $\Delta^{14}C$ is too small by an amount that cannot be accounted for by aliasing in the sampling. This discrepancy most likely indicates that the model's EUC is somewhat too diffusive.

As such, the modeling study serves two purposes. First, the control run provides a diagnostic test of model performance. Model skill in reproducing coral $\Delta^{14}C$ time series depends not only on the the local dynamical response of the equatorial ocean to wind forcing but also on many nonlocal processes, ranging from subduction in the subtropics to equatorward geostrophic flow within the thermocline to upwelling in the equatorial Pacific.

Second, the model results illustrate the way in which specific dynamical processes imprint themselves on the sea surface $\Delta^{14}C$ signal recorded by equatorial corals. The strong sensitivity to the opening of the Indonesian Throughflow indicates that the treatment of this boundary condition has far reaching consequences for tracer budgets in the equatorial thermocline. Also, the sensitivity of sea surface $\Delta^{14}C$ to interannual variability in wind stress forcing provides us with a tool to identify past variability in ocean circulation due to changes in wind forcing. The atmospheric $\Delta^{14}C$ forcing function (Figure 1) is smoothly varying in time, so the interannual $\Delta^{14}C$ variability recorded by corals can be used to identify past changes in ocean circulation.

In a future study we will use a global domain with similarly high meridional resolution in the tropics to address in more detail intergyre exchange between the South Pacific and the equatorial Pacific for the 40 year timescale between the beginning of the atmospheric testing of weapons and the World Ocean Circulation Experiment (WOCE) Pacific program. The expanded domain will not only allow us to address intergyre exchange in the South Pacific, but it will also allow us to study interbasin exchange of thermocline water between the Pacific and Indian Oceans.

Acknowledgments. We would like to thank Wally Broecker and Tom Guilderson for their constructive comments and suggestions. This work was supported by National Science Foundation contracts OCE-9633375 (Lamont-Doherty) and OCE-9796253 (Harvard University). This is Lamont-Doherty Earth Observatory contribution number 6017.

References

Aumont, O., J. C. Orr, P. Monfray, G. Madec, and E. Maier-Reimer, Nutrient trapping in the equatorial Pacific: The ocean circulation solution, *Global Biogeochem. Cycles, 13*, 351-369, 1999.

Broecker, W. S., T.-H. Peng, H. G. Ostlund, and M. Stuiver, The distribution of bomb radiocarbon in the ocean, *J. Geophys. Res., 90*, 6953-6970, 1985.

Broecker, W. S., S. Sutherland, W. Smethie, T.-H. Peng, and G. Ostlund, Oceanic radiocarbon: Separation of the natural and bomb components, *Global Biogeochem. Cycles, 9*, 263-288, 1995.

Craig, A. P., J. L. Bullister, D. E. Harrison, R. M. Chervin, and A. J. Semtner Jr., A comparison of temperature, salinity, and chlorofluorocarbon observations with results from a 1° resolution three-dimensional global ocean model, *J. Geophys Res., 103*, 1099-1119, 1998.

daSilva, A., C. Young, and S. Levitus, Atlas of surface marine data 1994, vol. 1, Algorithms and procedures, *NOAA Atlas NESDIS 6*, U.S. Dep. of Commer., Washington, D.C., 1994.

Deser, C., M. A. Alexander, and M. S. Timlin, Upper-ocean thermal variations in the North Pacific during 1970-1991, *J. Clim., 9*, 1840-1855, 1996.

Druffel, E., Bomb radiocarbon in the Pacific: Annual and seasonal timescale variations, *J. Mar. Res., 19*, 35-46, 1987.

Duffy, P., D. Eliason, A. Bourgeois, and C. Covey, Simulation of bomb radiocarbon in two global ocean general circulation models, *J. Geophys. Res., 100*, 22,545-22,563, 1995.

Follows, M. J., and J. C. Marshall, On models of bomb ^{14}C in the North Atlantic, *J. Geophys. Res., 101*, 22,577-22,582, 1996.

Gent, P. R., and M. A. Cane, A reduced gravity, primitive equation model of the upper equatorial ocean, *J. Comput. Phys., 81*, 444-480, 1989.

Gent, P. R., and J. C. McWilliams, Isopycnal mixing in ocean circulation models, *J. Phys. Oceanogr., 20*, 150-155, 1990.

Gibson, J. K., P. Kallber, S. Uppula, A. Hernandez, A. Nomura, and E. Serrano, ECMWF re-analysis project report series: ERA description, Tech. Rep., 1, 72 pp., Eur. Cent. for Medium Range Weather Forecasts, Reading, England, U.K., 1977.

Godfrey, J. S., The effect of the Indonesian throughflow on ocean circulation and heat exchange with the atmosphere: A review, *J. Geophys. Res., 101*, 12,217-12,237, 1996.

Gu, D., and S. G. H. Philander, Interdecadal climate fluctuations that depend on exchanges between the tropics and the extratropics, *Science, 275*, 805-807, 1997.

Guilderson, T., and D. P. Schrag, Abrupt shift in subsurface temperatures in the eastern tropical Pacific associated with recent changes in El Niño. *Science, 281*, 241-243, 1998.

Guilderson, T., D. P. Schrag, M. Kashgarian, and J. Southon, Radiocarbon variability in the western equatorial Pacific inferred from a high-resolution coral record from Nauru Island, *J. Geophys. Res., 103*, 24,641-24,650, 1998.

Griffies, S. M., The Gent-McWilliams skew-flux, *J. Phys. Oceanogr., 28*, 831-841, 1998.

Hazeleger, W., R. Seager, M. Visbeck., N. H. Naik, and K. B. Rodgers, On the impact of the midlatitude storm tracks on the upper Pacific Ocean, submitted to *J. Phys. Oceanogr.*, 1999.

Huang, R. X., and B. Qiu, Three-dimensional structure of the wind-driven circulation in the subtropical North Pacific, *J. Phys. Oceanogr., 24*, 1608-1622, 1994.

Kaplan, A., M. Cane, Y. Kushnir, A. Clement, M. Blumenthal, and B. Rajagopalan, Analyses of global sea surface temperature 1856-1991, *J. Geophys. Res., 103*, 18,567-18,589, 1998 .

Large, W. G., G. Danabasoglu, S. C. Doney, and J. C. McWilliams, Sensitivity to surface forcing and boundary

layer mixing in a global ocean model: Annual-mean climatology, *J. Phys. Oceanogr.*, *27*, 2418-2447, 1997.

Levitus, S., and T. P. Boyer, *World Ocean Atlas 1994*, vol. 4, *Temperature*, 117 pp., U.S. Dep. of Commer., Washington, D. C., 1994.

Li, Z., and H. G. Leighton, Global climatologies of the solar radiation budgets at the surface and in the atmosphere for 5 years of ERBE data, *J. Geophys. Res.*, *98*, 4919-4930, 1993.

Linick, T. W., La Jolla measurements of radiocarbon in the oceans, *Radiocarbon*, *20*, 333-359, 1978.

Moore, M., D. Schrag, and M. Kashgarian, Coral radiocarbon constraints on the source of the Indonesian throughflow, *J. Geophys. Res.*, *102*, 12,359-12,365, 1997.

Naik, N., M. A. Cane, S. Basin, and M. Israeli, A solver for the barotropic mode in the presence of variable topography and islands, *Mon. Weather Rev.*, *123*, 817-832, 1995.

Ostlund, H., and M. Stuiver, GEOSECS Pacific radiocarbon, *Radiocarbon*, *22*, 25-53, 1980.

Pacanowski, R. C., and S. G. Philander, Parameterization of vertical mixing in numerical models of the tropical oceans, *J. Phys. Oceanogr.*, *11*, 1443-1531, 1981.

Quay, P. D., M. Stuiver, and W. S. Broecker, Upwelling rates for the equatorial Pacific Ocean derived from the bomb ^{14}C distribution. *J.Mar.Res.*, *41*, 769-793, 1983.

Rodgers, K. B., M. A. Cane, and D. P. Schrag, Seasonal variability of sea surface $\Delta^{14}C$ in the equatorial Pacific in an ocean circulation model, *J. Geophys. Res.*, *102*, 18,627-18,639, 1997.

Rodgers, K. B., M. A. Cane, N. H. Naik, and D. P. Schrag, The role of the Indonesian Throughflow in equatorial Pacific thermocline ventilation, *J. Geophys. Res.*, *104*, 20,551-20,570, 1999.

Rossow, W. B., and R. A. Schiffer, ISCCP cloud data products. *Bull. Am. Meteorol. Soc.*, *72*, 2-20, 1991.

Sarmiento, J. L., and K. Bryan, An ocean transport model for the North Atlantic, *J. Geophys. Res.*, *87*, 394-408, 1982.

Seager, R., M. B. Blumenthal, and Y. Kushnir, An advective atmospheric mixed layer model for ocean modeling purposes: Global simulation of surface heat fluxes. *J. Clim.*, **8**, 1951-1964, 1995.

Shapiro, R., Smoothing, filtering, and boundary effects, *Rev. Geophys.*, , *8*, 359-387, 1970.

Stuiver, M., P. D. Quay, and H. G. Ostlund, Abyssal water carbon-14 distribution and the age of the world oceans, *Science*, *219*, 849-851, 1983.

Toggweiler, J. R., A six zone regionalized model for bomb radiocarbon and CO_2 in the upper kilometer of the Pacific Ocean, Ph.D. thesis, Columbia Univ., New York, 1983.

Toggweiler, J. R., K. Dixon, and K. Bryan, Simulations of radiocarbon in a coarse-resolution, world ocean model, 1, Steady state, prebomb distribution, *J. Geophys. Res.*, , *94*, 8217-8242, 1989a.

Toggweiler, J. R., K. Dixon, and K. Bryan, Simulations of radiocarbon in a coarse-resolution, world ocean model, 2, Distribution of bomb-produced ^{14}C, *J. Geophys. Res.*, , *94*, 8243-8264, 1989b.

Toggweiler, J. R., K. Dixon, and W. S. Broecker, The Peru upwelling and the ventilation of the South Pacific thermocline, *J. Geophys. Res.*, , *96*, 20,467-20,497, 1991.

Tsuchiya, M., The origin of the Pacific equatorial 13° water, *J. Phys. Oceanogr.*, *11*, 794-812, 1981.

Wyrtki, K., An estimate of equatorial upwelling in the Pacific, *J. Phys. Oceanogr.*, *11*, 1205-1214, 1981.

Zhang, R.-H., L. M. Rothstein, and A. J. Busalacchi, Origin of upper-ocean warming and El Niño changes in the tropical Pacific Ocean, *Nature*, *391*, 879-883, 1998.

K.B. Rodgers, Max-Planck-Institut für Meteorologie, Bundesstrasse 55, D-20146 Hamburg, Germany. (e-mail: rodgers@dkrz.de)

D.P. Schrag, Department of Earth and Planetary Sciences, Harvard University, Cambridge, Massachusetts, 02138. (e-mail: schrag@eps.harvard.edu)

M.A. Cane and N. Naik, Lamont-Doherty Earth Observatory, Columbia University, Palisades, New York, 10964. (e-mail: mcane@ldeo.columbia.edu and naomi@ldeo.columbia.edu)

(Received June 30, 1998; revised June 1, 1999; accepted July 30, 1999.)